https://ntrs.nasa.gov/search.jsp?R=19660011744 2020-03-24T02:57:42+00:00Z

NASA TECHNICAL NOTE

NASA TN D-3366

NASA TN D-3366

FACILITY FORM 602

N66-21033
(ACCESSION NUMBER)

(THRU)

58
(PAGES)

1
(CODE)

(NASA CR OR TMX OR AD NUMBER)

30
(CATEGORY)

ANGLE-OF-ATTACK ANALYSIS FOR PROJECT FIRE 1 PAYLOAD REENTRY FLIGHT

by Gerard E. Woodbury

Langley Research Center

Langley Station, Hampton, Va.

GPO PRICE $

CFSTI PRICE(S) $ .85

Hard copy (HC)

Microfiche (MF) .50

ff 653 July 65

NATIONAL AERONAUTICS AND SPACE ADMINISTRATION • WASHINGTON, D. C. • APRIL 1966

NASA TN D-3366

ANGLE-OF-ATTACK ANALYSIS FOR PROJECT FIRE 1 PAYLOAD REENTRY FLIGHT

By Gerard E. Woodbury

Langley Research Center
Langley Station, Hampton, Va.

NATIONAL AERONAUTICS AND SPACE ADMINISTRATION

For sale by the Clearinghouse for Federal Scientific and Technical Information
Springfield, Virginia 22151 – Price $0.85

ANGLE-OF-ATTACK ANALYSIS FOR PROJECT FIRE 1 PAYLOAD REENTRY FLIGHT

By Gerard E. Woodbury
Langley Research Center

SUMMARY

21033

An investigation of the flight motions of the Project Fire 1 payload was made through the use of digital-computer simulation techniques since limited motion instrument data did not permit more direct methods of analysis. The simulations were obtained from a six-degree-of-freedom computer program which numerically solved the equations of motion. The complete nonlinear wind-tunnel data and calculated time histories of the mass characteristics of the body were used in the program. The only data available for simulation consisted of continuous data from the yaw-rate gyro and commutated accelerometer data. Some of the rate-gyro data were lost, however, since the excursions of the rate gyro oscillations exceeded calibration limits. Also, periodic fadeout of the telemetry system caused a loss of both rate-gyro and accelerometer data. A separate study was necessary to obtain the initial conditions for the simulations. This study consisted of a curve-fit program which used the angular-rate-history solution to the linearized equations of motion to approximate the pitch rate from measurements of the yaw-rate gyro. Since the resultant force and resultant pitching-moment coefficients of the wind-tunnel aerodynamics were linear up to angles of attack of 35°, this curve-fit program could be used. With the initial angular velocities and accelerations obtained at a selected time from the curve-fit program, all the remaining initial conditions, with exception of the trajectory quantities, necessary to start an exact solution on the six-degree-of-freedom computer program were easily determined. The purpose of this investigation was to determine the angle-of-attack and motion histories of the reentry package during the heating data period of the Project Fire 1 experiment. The reentry package experienced a disturbance at about 1666 seconds of elapsed flight time at an altitude of approximately 69 800 meters and a velocity of about 11 500 meters per sec. Prior to the disturbance, the body was coning with a half-angle of about 1°.

The results of the analysis indicated that the angle-of-attack envelope increased to about 33° after the disturbance. The factors which caused the disturbance could not be isolated. The angle-of-attack envelope damped from 33° to about 13° at maximum dynamic pressure. The roll rate was initially 18.85 radians/sec. The motion patterns

of the body were typical of those for bodies which are statically stable and have roll-to-pitch inertia ratios greater than 1. The simulations indicated that trim was small.

INTRODUCTION

Project Fire is a National Aeronautics and Space Administration research effort to obtain heating data on a blunt Apollo shaped reentry body at hyperbolic velocities. The first flight test, Fire 1, was launched 14 April 1964, from Cape Kennedy, Florida. Approximately halfway through reentry the payload experienced a large unexpected disturbance which caused severe motions to ensue. Reference 1 presents a preliminary analysis of the heating data obtained from Fire 1 and points out the need for an analysis of the body motions after the disturbance to assess their effect on the interpretation of the heating data. References 2 and 3 define the flight trajectory and atmospheric environment and describe the mechanical hardware of Fire 1.

Payload performance and stability instrumentation consisted of three rate gyros and three linear accelerometers. During reentry these instruments indicated small coning half-angles of about 1^{o} which were initiated by the separation impulse. The analysis of the body motions after the large disturbance at approximately 1666 sec was complicated by the fact that (1) the roll- and pitch-rate gyros became inoperative, (2) the linear accelerometers were not located on the center of gravity and their outputs were not continuous, but rather were commutated, (3) the telemetry experienced periodic noise disturbances, (4) the reentry package was lost by radar shortly after the onset of telemetry blackout, and (5) the excursions of the yaw-rate-gyro-data oscillations exceeded calibration limits.

There were seven intervals on the telemeter oscillograph records during reentry that were free of noise interference. The present study is limited to analysis of these seven periods. The primary purpose of this study is to analyze the motions and determine the magnitude and frequencies of the angle of attack during the heating data period. In addition, the study was made to substantiate the trajectory parameters determined in the study of reference 2.

In general, simulation techniques employing aerodynamic data obtained from wind-tunnel tests and solutions to the equations of motion as obtained from digital-computer programs were used to analyze the motion data. The ranges of velocity and altitude of the simulations were from about 11 430 meters per sec at approximately 63 400 meters to 2 800 meters per sec at 33 070 meters.

SYMBOLS

A_N	normal acceleration, $-A_Z$, g units
A_R	resultant acceleration in Y_b-Z_b body-axis plane, $\sqrt{A_Y^2 + A_Z^2}$, g units
A_X, A_Y, A_Z	accelerations parallel to X_b, Y_b, and Z_b body axes, respectively, g units
$C_{N_\alpha} = C_{R_\eta} = \frac{\partial C_R}{\partial \eta}$	resultant- or normal-force-curve slope
C_R	resultant force coefficient in body-axis system
C_X	force coefficient along X_b body axis
C_{Y_o}, C_{Z_o}	force coefficients due to asymmetry along Y_b and Z_b body axes, respectively
C_m	resultant pitching-moment coefficient in Y_b-Z_b body-axis plane
$C_{m_\alpha} = C_{m_\eta} = \frac{\partial C_m}{\partial \eta}$	pitching-moment-curve slope
$C_{m_q} = \frac{\partial C_m}{\partial\left(\frac{qd}{2\bar{V}}\right)}$	moment coefficient about Y_b body axis due to pitching velocity
d	reference diameter, meters
$d_H = \lambda_o + \Delta\lambda$	high damping rate, 1/sec
$d_L = \lambda_o - \Delta\lambda$	low damping rate, 1/sec
e	base of Napierian logarithm
F_X, F_Y, F_Z	force components along X_b, Y_b, and Z_b body axes, respectively, newtons
g	acceleration due to gravity, meters/sec^2

h	altitude, meters
I_X	mass moment of inertia about X_b body axis, kilogram-meters^2
I	mass moment of inertia about Y_b and Z_b body axes, kilogram-meters^2
$I' = \frac{I}{\bar{q}Sd}$, sec^2	
$i = \sqrt{-1}$	
K_1, K_2, K_3, K_4	constants in angular-rate solution of linearized equations of motion
M_Y, M_Z	moments about the Y_b and Z_b body axes, respectively, newton-meters
m	mass, kilograms
$m' = \frac{mu}{\bar{q}S}$, sec	
$\bar{q}$	dynamic pressure, newtons/meter^2
p, q, r	angular velocities about the X_b, Y_b, and Z_b body axes, respectively, radians/sec
R_1, R_2	initial magnitudes of rotating vectors of epicyclic motion
S	reference area, meters^2
t	elapsed flight time, sec
Δt_n	time used in equations (1) and (2), $t_n - t_1$, sec
u, v, w	inertial velocity components along X_b, Y_b, and Z_b body axes, respectively, meters/sec
$\bar{u}, \bar{v}, \bar{w}$	earth-relative velocity components along X_b, Y_b, and Z_b body axes, respectively, meters/sec

$\overline{V}$	earth-relative velocity, meters/sec
X_b, Y_b, Z_b	orthogonal body-axis system with origin at center of gravity
X_g, Y_g, Z_g	orthogonal gravity-axis system with origin at center of gravity
x	longitudinal location of accelerometer measured from Fire station 0 (see fig. 2), meters
x_{cg}	longitudinal position of center of gravity measured from Fire station 0, meters
x_o	longitudinal position of center of pressure of asymmetric force, meters
x_x, y_x, z_x	displacements between longitudinal accelerometer (A_X) and center of gravity parallel to X_b, Y_b, and Z_b body axes, respectively, meters
x_y, y_y, z_y	displacements between transverse accelerometer (A_Y) and center of gravity parallel to X_b, Y_b, and Z_b body axes, respectively, meters
x_z, y_z, z_z	displacements between normal accelerometer (A_Z) and center of gravity parallel to X_b, Y_b, and Z_b body axes, respectively, meters
y_b, z_b	coordinates along Y_b and Z_b body axes, respectively, meters
α	angle of attack, deg
β	angle of yaw, deg
η	total angle of attack, deg
γ_p	earth-relative flight-path angle, deg
γ_y	earth-relative heading, deg

θ, ψ, φ	body attitude angles relative to gravity-axis system, deg
φ'	aerodynamic phase angle, deg
λ_o	nonrolling damping rate, per sec
$\Delta\lambda$	damping rate due to roll, per sec
ν_1, ν_2	initial angular orientation of rotating vectors, radians
ρ	air density, kilograms/meter^3
ω_H	high frequency, $\omega_o + \Delta\omega$, radians/sec
ω_L	low frequency, $\omega_o - \Delta\omega$, radians/sec
ω_n	natural pitch frequency, radians/sec
ω_o	basic oscillation frequency, radians/sec
$\Delta\omega$	component of total pitch frequency resulting directly from roll, radians/sec

$\Omega = q + ir$

Subscripts:

o	initial conditions (unless defined differently elsewhere)
max	maximum condition
trim	trim condition
cg	center-of-gravity value
i	indicated instrument value

A dot over a symbol denotes differentiation with respect to time.

TEST AND MEASUREMENTS

In general, the Project Fire 1 vehicle consisted of an Atlas launch vehicle, a velocity package containing an Antares II-A5 rocket motor, and the reentry package which contained the experimental apparatus. The reentry package was a blunt Apollo shaped body with a unique composite heat shield made up of two ejectable phenolic-asbestos layers sandwiched between three beryllium calorimeters which allowed three separate measurements of the heat pulse to be made during reentry.

The Atlas put the Fire 1 spacecraft (combination of velocity and reentry packages) into a precise ballistic trajectory along the Atlantic Missile Range. After separation from the Atlas, the spacecraft was oriented to the proper Antares ignition attitude by the velocity-package control system and was spun up to approximately 18.85 radians/sec for spin stabilization. Sometime after burnout of the Antares rocket, the reentry package was cold-separated from the velocity package by a spring mechanism and reentered the earth's atmosphere at 11 574 meters per sec at an altitude of 121 920 meters and approximately 8 028 kilometers downrange near Ascension Island. A more detailed description of the vehicle and flight events may be found in references 2 and 3.

Flight Tests

The sequence of significant flight events during reentry are listed in table 1. The reentry package separated from the velocity package at $t = 1640.5$ seconds. Approximately 26 seconds later an unexpected disturbance occurred and large motions ensued. The trajectory was confirmed by radar until radar blackout at $t = 1660.2$ seconds. The latter part of the trajectory was extended by particle trajectory computer programs as in references 2 and 3. These extensions, however, were only used as a guide in the motion analysis.

The motion instrumentation in the payload consisted of three rate gyros and three linear accelerometers. After the disturbance ($t \approx 1666$ sec), the amplitudes of the yaw rate exceeded the range of the yaw-rate gyro. The roll-rate gyro was inoperative and the pitch rate-gyro operated erratically. All the accelerometer data were commutated. The accelerometers also were located well off the center of gravity and consequently measured accelerations due to angular velocity and angular accelerations as well as the translatory accelerations of the vehicle. The ranges of all the instruments, together with the locations of the accelerometers, are listed in table 2. Details of other reentry-package instrumentation such as calorimeters and thermocouples are given in references 1 to 3. A photograph showing the reentry portion of the telemeter oscillograph record (after the disturbance) is shown in figure 1. The seven data intervals free of noise interference are clearly shown in the figure. It may be noted that differences exist both in the amount of

noise and the time various events occur on the two playback records. The noise difference is probably due to the arbitrary nature of the telemetry decay. The time difference is slight, on the order of 0.03 second, and is probably a result of a time lag in the playback system. The data of the second playback are included in the analysis since it provided some data not available on the first playback. Since there was an overlapping of data in all cases where data from the second playback were used, the time difference was easily discerned and compensated for by shifting the time scale of the second playback data to make the overlapping portions congruent.

Physical Characteristics and Ground Tests

A sketch of the Project Fire 1 payload (reentry package) is shown in figure 2(a) and a sketch of a similar configuration which was tested in various facilities of the NASA wind-tunnel complex is shown in figure 2(b). In general, the overall linear and angular dimensions of the two bodies were similar; however, a prime difference was in the curvature and edge of the face of the wind-tunnel test model. The physical properties of the flight model are presented in tabular form in figure 2 and are illustrated graphically in figure 3. The wind-tunnel data employed for the reentry analysis are presented in figure 4 for angles of attack from 0 to 80°. These data are averaged from data obtained during tests at a Mach number of 4.65 (ref. 4) and from unpublished wind-tunnel data at Mach numbers of 5, 7.3, and 9. The moment center was determined by the equations shown in figure 2. The aerodynamic reference area and length were based on the model frontal area and diameter, respectively.

Exploratory wind-tunnel tests were also made after the flight to determine whether reasonable amounts of uneven heat erosion of materials on the face of the reentry package and/or disturbances from unsymmetrical ejection of heat-shield segments could have induced aerodynamic forces and moments of the order to cause the aforementioned disturbance. Models were tested with various combinations of pie-shaped sections removed from their faces for this purpose. No significant change in the static aerodynamic coefficients was found. Only the wind-tunnel data used in the analysis of the motions of the reentry package are presented in this paper.

METHOD OF ANALYSIS

Simulation techniques were used in the motion analysis since incomplete rate-gyro data did not permit more direct methods of workup. A block diagram summarizing the techniques employed in the analysis of the Fire 1 data is shown in figure 5. In general, the simulations were made to match the on-scale data frequencies and amplitudes. In order to start the simulations, a separate study shown on the left side of the block diagram was first necessary to approximate required initial conditions of the variables not

measured. Once these conditions were determined, the simulation calculations were obtained with a six-degree-of-freedom computer program as shown on the right side of the block diagram. There were seven data periods. Each motion simulation was essentially independent of the other data periods.

Motion Initial Conditions

It should be noted in figure 4 that the pitching-moment coefficient is linear up to angle of attack of about 35°. Thus, a curve-fit program using the angular-rate-history solution to the linearized equations of motion was set up to approximate the pitch rate from measurements made by the yaw-rate gyro. The principal steps in the derivation of this solution are presented in appendix A. The derivation is based on that of reference 5, which presents the angle-of-attack-history solution for the linearized equations. By substituting the angle-of-attack solution in the linearized force equation of reference 5 and solving for the angular rates, the following forms for the rate-gyro equations were obtained:

$$r = K_1 \sin \omega_L t + K_2 \cos \omega_L t + K_3 \sin \omega_H t + K_4 \cos \omega_H t \tag{1}$$

$$q = -K_2 \sin \omega_L t + K_1 \cos \omega_L t + K_4 \sin \omega_H t - K_3 \cos \omega_H t \tag{2}$$

where t is equal to Δt_n.

These equations are written in terms of the body-axis system for a body with 90° rotational and mass symmetry and negligible trim angles. The body-axis system is shown in figure 6. It is assumed that free-stream conditions are constant due to the brevity of each data period. All damping factors are neglected because of the high speed during the period of the analysis. Although the errors due to large angles of attack would have some effect on the accuracy of the linearized analysis, it was found that the utilization of the linear solution for obtaining approximate initial conditions for the exact calculations was justified on the basis that iterations could be performed if required in the final simulations.

Basically, the linear solution is written in terms of the algebraic sum of two sine waves of different amplitudes, frequencies, and initial phase angles, and may be represented by the epicyclic motion of two rotating vector arms revolving at different rates. There are six unknowns $(K_1, K_2, K_3, K_4, \omega_L$, and $\omega_H)$ to be determined in the analysis of each data period. First, the frequencies ω_L and ω_H of the two rotating arms are computed from estimated values of relative velocity, dynamic pressure, roll rate, vehicle mass characteristics, and linear wind-tunnel aerodynamics (shown in eqs. (A9), (A10), (A14), (A22), and (A23)). These frequencies plus four values of yaw-rate data

chosen from within the first data cycle to be fitted were substituted in equation (1) to yield four simultaneous equations. The remaining unknowns or constants were evaluated from the solution of these four equations. The yaw rate is then generated from equation (1) and compared with a corresponding portion of the flight record. This procedure may be iterated by changing the estimated frequencies slightly, until a very close match is obtained. The time interval selected for curve fitting should be limited to keep the assumption of constant free-stream conditions valid. Finally, the constants were substituted in equation (2) to obtain the corresponding pitch-rate history. Equations (1) and (2) were differentiated to obtain the angular accelerations of the vehicle. With these angular-velocity and acceleration histories, all the remaining initial conditions, with exception of the trajectory quantities, necessary to start an exact solution using a six-degree-of-freedom computer program may be determined; a description of the procedure is presented in appendix A.

Simulations

The six-degree-of-freedom computer program is presented in reference 6; only those equations relative to generating the motion patterns are presented in appendix B. This program represents the exact solution to the equations of motion for six degrees of freedom. However, it is only exact to the degree required by the user. In the present instance, for example, the damping was neglected for the same reasons the damping was neglected in the curve-fit program. The exact program determines both translatory and rotational motions of a rigid body in three-dimensional space. Gravity effects and position were computed relative to an oblate spheroidal earth with a 1962 Standard Atmosphere (ref. 7). The variation with time of the center of gravity, mass, moments of inertia, reference areas and diameters, plus the complete nonlinear aerodynamic coefficients as presented in figures 2, 3, and 4, was programed. An option was added to this program to calculate the accelerations of an arbitrary point on the body. This option was added to simulate accelerometer data of instruments which had been located off the center of gravity of the reentry package (eqs. (B14), (B15), and (B16)).

With given aerodynamic and mass characteristics, the high and low frequencies determined for each data interval by the curve-fit program were transformed to those quantities with which the exact program works in terms of – namely, $\bar{q}$ and p. This transformation was made through the use of equations (A24) and (A25). Subsequently, values of $\overline{V}$ and ρ were determined to satisfy the derived value of $\bar{q}$. For simulation of the first data interval, $\overline{V}$ was obtained directly from the extension of the flight trajectory of reference 3 since it was believed that $\overline{V}$ was less sensitive to possible errors in that trajectory at the onset of reentry. The required air density ρ was determined by solving a rewritten form of the usual $\bar{q}$ expression, $\frac{1}{2}\rho\overline{V}^2$. By referring to

the U.S. Standard Atmosphere, 1962 (ref. 7), an initial altitude was then selected. A minimum of two simulation runs were made in the data period by using the same initial velocity and altitude, but slightly different flight-path angles, and continued through the adjoining noise interference interval to the starting time of the next data period. This procedure was used to aid in determining the combination of velocity, altitude, and flight-path angle which would again satisfy the $\bar{q}$ requirement determined by the curve-fit program in the latter data period. This procedure was repeated for each of the remaining data periods.

Once the data curves were matched, the computed histories of α, β, η, θ, and ψ were assumed to represent the flight motions and conditions and were used as a basis for a radiative-heating analysis of the Fire 1 payload (ref. 8).

RESULTS AND DISCUSSION

Basic Data

Comparisons of the basic flight data with the numerical solution of the six-degree-of-freedom program for a portion of each data interval are presented in figures 7 to 13. The symbols in the rate-gyro curves represent selected points taken at constant intervals from continuous data, whereas the symbols on the acceleration curves indicate the commutated data. Flagged symbols represent data from a different playback of the record. The portion of the record presented represents virtually all the clear data in the interval. The comparisons include those of r, $A_{Y,i}$, and $A_{Z,i}$, plus one of q in the last period ($t \approx 1687$ sec) when it appeared the pitch-rate gyro might be operating properly. Also presented is a comparison of the generated yaw rate from the linear solution of the curve-fit program with flight and numerical computation values in the first period (see fig. 7(a)). This case is typical and more comparisons are not presented. A summary of the four data points selected from each data interval for the curve-fit program is presented in table 3 together with the resultant frequencies and amplitude constants obtained therefrom. Likewise, a summary of the initial conditions used in the exact solution of the computer program is presented in table 4.

Simulations

In general, the comparison in figures 7 to 13 shows that there is good agreement between the simulations and flight data as to amplitudes and frequencies. The simulation frequencies, in particular, are very close to those of the data. There is no direct way to compare the peaks of the amplitudes of either the rate-gyro or accelerometer data since the angular rates exceeded the calibration of rate gyros and the data of the accelerometers were commutated. Histories of the missing data beyond the limits of the yaw-rate

gyro were computed and are considered valid since close agreement was obtained with preceding and following on-scale data. The simulated values of $A_{Y,i}$ and $A_{Z,i}$ provided the only continuous accelerometer variation, without which it would have been most difficult to make valid fairings of the commutated flight data. The techniques used in the analysis of the accelerometer data were necessary for two reasons: (1) each accelerometer was located separately at different distances from the center of gravity and thus measured accelerations due to angular rates and accelerations (see appendix B) in addition to the accelerations of the center of gravity and (2) since $A_{Z,i}$ and $A_{Y,i}$ were commutated, their recorded values necessarily occurred at different times; hence, direct computation of the resultant total acceleration A_R and the total normal-force coefficient C_R would have been most difficult.

The good agreement between the curve-fit-program curve and the numerical-solution curve (fig. 7(a)) is due primarily to the linearity of the C_R and C_m wind-tunnel data up to angles of attack of 35^o. Trim forces and moments due to aerodynamic and mass asymmetries were neglected in the simulation of the accelerometer and rate-gyro data. The good agreement between the numerical solution and the flight data (fig. 7(a)), therefore, indicates that η_{trim} of the flight vehicle was small.

Two significant parameters, $\Delta\omega$ and ω_o, were isolated from the simulations and their variations with time are presented in figure 14. By neglecting the damping effects during small time intervals, it was possible to solve the expressions for these frequency parameters for roll rate p and the product $C_{m_\alpha}\bar{q}$. It was thought the roll rate would remain constant throughout the flight since the reentry package was a symmetrical body of revolution with no fins to provide rapid roll damping. However, it was found from the curve-fit program and validated by the exact program that p was initially 18.85 radians/sec and generally decreased with time. This roll-rate deceleration was probably caused by such factors as skin-friction roll damping and the effects of possible heat erosion on the rolling moment. It may be noted that the dropoff of p with time was not uniform (see table 4) and was probably the result of sudden changes in mass characteristics and nose shape when the phenolic-asbestos heat shields were ejected ($t \approx 1670$ and 1676 sec). A study of the effects of inertia was not made since preliminary estimates showed that practical errors in I_X and I would have only a small effect on the frequencies. Therefore, the aforementioned iterations were concentrated on finding values of rolling velocity and natural pitch frequency required to match the flight data.

The variations of pitching-moment-curve slope, based on the wind-tunnel data (see section entitled "Physical Characteristics and Ground Test") adjusted for reentry package center-of-gravity location referred to the wind-tunnel model, are shown in figure 15(a). The corresponding values of dynamic pressure employed in the simulation runs (table 4) are presented and compared with dynamic-pressure calculations from a ballistic

trajectory of reference 3 and a modified ballistic trajectory from reference 2 in figure 15(b). The modified trajectory was computed by using drag coefficients based on the average angle of attack determined from the present report. The differences shown in $\bar{q}$ from the three methods are not significantly large and may be accounted for by experimental errors in either the flight data or the wind-tunnel tests, or both.

Angles of Attack

The motion patterns in the inertial plane (θ, ψ) at selected flight intervals are presented in figure 16. The representative altitudes and relative velocities for the starting time of each pattern are listed in table 4. Each interval is approximately 1 second long; hence, changes in altitude and velocity were small, and as a result, the pattern in each interval shown is generally symmetrical. However, the patterns are changing gradually with time. The patterns are typical of those for statically stable bodies which have roll-to-pitch inertia ratios greater than 1 $\left(\frac{I_X}{I} > 1\right)$, inasmuch as such bodies always have below-resonance motions characterized by outside loops. The center of the inertial patterns is approximately the projected velocity vector defined by its two flight-path angles, γ_p and γ_y. The radial distance between the center of each pattern and the curves is approximately the resultant angle of attack. A comparison of the successive peaks in each pattern shows that the damping is small; the amount of damping or divergence indicated in successive patterns is due to the dynamic-pressure gradient since $C_{m_q} = 0$ in the calculations.

The motion patterns in the relative plane (α, β) at selected flight intervals are presented in figure 17. These motions are symmetrical about the origin ($\alpha = 0$, $\beta = 0$) since trim effects were zeroed. The radial distance from the origin to the curve is again approximately the total angle of attack. The effects of damping are similar to those noted previously. The difference between the relative and inertial patterns lies in the axis system to which each is referred. The relative motions are referred to the body-axis system which rotates with the body at its roll rate. The inertial motions are referred to the gravity-axis system which rotates only with respect to an inertial reference, as the body moves over the earth.

The total angle-of-attack envelope is presented in figure 18 and shows the maximum and minimum bounds of its oscillations. Until $t \approx 1666$ seconds, the reentry package was coning with 1° half-angle cone thought to be caused by tipoff impulses at separation from the velocity package. A disturbance was experienced at $t \approx 1666$ seconds. (See fig. 1.) Based on the calculated coning-motion buildup thereafter, a resultant momentum impulse of about 19.4 newtons-meter-sec would have been required to increase the total angle-of-attack oscillations from 1° to about 33°. No attempt was made to analyze this disturbance further since the continuous data from the yaw-rate gyro experienced considerable noise

interference shortly after the disturbance. The upper bound of the η envelope decreased to a minimum of about 13° at approximately $\bar{q}_{max}$ and then increased gradually as the dynamic pressure decreased. This angle-of-attack envelope is the one on which the modified ballistic trajectory of reference 2 is based.

CONCLUDING REMARKS

An analysis of the flight motions of the Project Fire 1 payload was made by a digital-computer simulation of the rate-gyro and accelerometer data. This method of analysis was necessary since limited instrument data, consisting of continuous data from only the yaw-rate gyro, and commutated accelerometer data were available. The purpose of this analysis was to determine the angle-of-attack and motion histories of the reentry package during the experiment portion of the flight. The simulations were obtained from a six-degree-of-freedom computer program which numerically solved the equations of motion. The complete nonlinear wind-tunnel aerodynamics and calculated time histories of the mass characteristics of the body were used in the computer program. The reentry package experienced a disturbance at about 1666 seconds of elapsed flight time at an altitude of approximately 69 800 meters and a velocity of about 11 500 meters per sec. Just before the disturbance, the body was coning with a half-angle of about 1°. The results of the analysis indicate the following:

(1) After the disturbance, the angle-of-attack envelope increased from 1° to a maximum of about 33°, subsequently damped to a minimum of about 13° at maximum dynamic pressure, and increased somewhat thereafter as dynamic pressure decreased. While the factors which caused the disturbance could not be isolated, it was determined that a resultant momentum impulse of about 19.4 newton-meters-sec would have been required to produce this change in the magnitude of the motions.

(2) The roll rate was initially 18.85 radians/sec and decreased slightly during the experiment portion of the flight.

(3) The motion patterns of the reentry package were typical of those for bodies which are statically stable and have roll-to-pitch inertia ratios greater than 1.

(4) Total angle-of-attack trim was small.

Langley Research Center,
National Aeronautics and Space Administration,
Langley Station, Hampton, Va., November 17, 1965.

APPENDIX A

ANGULAR-RATE SOLUTION OF THE LINEARIZED EQUATIONS OF MOTION AND APPLICATION FOR OBTAINING INITIAL CONDITIONS FOR SIMULATION OF FLIGHT

Angular-Rate Solution of the Linearized Equations of Motion

The assumptions made for linearizing the equations of motion for a spinning symmetrical missile with respect to the body-axis system (fig. 6) are as follows:

(1) Constant free-stream conditions exist.

(2) The missile has constant rolling velocity.

(3) Aerodynamic damping forces and gravitational forces are negligible in comparison with forces due to angle of attack and angle of sideslip.

(4) Small angle approximations are valid.

(5) Magnus forces and moments are negligible.

The equations of motion reduce to the following four expressions:

$$\dot{\beta} + r - p\alpha = \frac{-C_{N_\alpha}\beta\bar{q}S + C_{Y_o}\bar{q}S}{mu} = \frac{\Sigma F_Y}{mu} \tag{A1}$$

$$\dot{\alpha} - q + p\beta = \frac{-C_{N_\alpha}\alpha\bar{q}S + C_{Z_o}\bar{q}S}{mu} = \frac{\Sigma F_Z}{mu} \tag{A2}$$

$$\dot{q}I - pr(I - I_X) = C_{m_\alpha}\alpha\bar{q}Sd + C_{m_q}\left(\frac{qd}{2\bar{V}}\right)\bar{q}Sd - C_{Z_o}\bar{q}Sx_o = \Sigma M_Y \tag{A3}$$

$$\dot{r}I + pq(I - I_X) = -C_{m_\alpha}\beta\bar{q}Sd + C_{m_q}\left(\frac{rd}{2\bar{V}}\right)\bar{q}Sd + C_{Y_o}\bar{q}Sx_o = \Sigma M_Z \tag{A4}$$

The solution of these linearized equations for total angle of attack η is given in reference 5 and by changing some symbols for convenience and clarity becomes:

$$\eta = \eta_{trim} + R_1 e^{i\nu_{1_e}(d_H + i\omega_L)t} + R_2 e^{i\nu_{2_e}(d_L - i\omega_H)t} \tag{A5}$$

where in reference 5:

$$\eta = \beta + i\alpha \tag{A6}$$

$$d_H = \lambda_o + \Delta\lambda \tag{A7}$$

$$d_L = \lambda_o - \Delta\lambda \tag{A8}$$

$$\omega_H = \omega_o + \Delta\omega \tag{A9}$$

$$\omega_L = \omega_o - \Delta\omega \tag{A10}$$

and

$$\lambda_o = -\frac{1}{2}\left(\frac{C_{N_\alpha}}{m'} - \frac{C_{m_q}}{I'}\right) \tag{A11}$$

$$\omega_o = \frac{1}{2\sqrt{2}}\sqrt{-\frac{4C_{m_\alpha}}{I'} + p^2\frac{I_X^2}{I^2} - \left(\frac{C_{N_\alpha}}{m'} + \frac{C_{m_q}}{I'}\right)^2 + \sqrt{\left[-\frac{4C_{m_\alpha}}{I'} + p^2\frac{I_X^2}{I^2} - \left(\frac{C_{N_\alpha}}{m'} + \frac{C_{m_q}}{I'}\right)^2\right]^2 + 4\left[p\frac{I_X}{I}\left(\frac{C_{N_\alpha}}{m'} + \frac{C_{m_q}}{I'}\right)\right]^2}} \tag{A12}$$

$$\Delta\lambda = \frac{1}{4\omega_o}\, p\, \frac{I_X}{I}\left(\frac{C_{N_\alpha}}{m'} + \frac{C_{m_q}}{I'}\right) \tag{A13}$$

$$\Delta\omega = p\left(1 - \frac{I_X}{2I}\right) \tag{A14}$$

Equations (A1) and (A2) may be combined by the use of complex numbers, and reduced, by letting $\Omega = q + ir$ and $m' = \frac{mu}{\bar{q}S}$, to the following form:

$$\dot{\eta} + ip\eta - i\Omega = \frac{-C_{N_\alpha}\eta}{m'} + \frac{C_{Y_o} + iC_{Z_o}}{m'} \tag{A15}$$

The angle-of-attack solution given in equation (A5) was substituted in the force equation (eq. (A15)) to yield the following solution for the angular rate:

$$\Omega = q + ir = \left[p + \omega_L - i\left(d_H + \frac{C_{N_\alpha}}{m'}\right)\right] R_1 e^{d_H t + i(\omega_L t + \nu_1)}$$

$$+ \left[p - \omega_H - i\left(d_L + \frac{C_{N_\alpha}}{m'}\right)\right] R_2 e^{d_L t - i(\omega_H t - \nu_2)} + \left(p - i\frac{C_{N_\alpha}}{m'}\right)\eta_{trim} + \frac{i(C_{Y_o} + iC_{Z_o})}{m'} \tag{A16}$$

By using the relation $e^{i\tau} = \cos\tau + i \sin\tau$, the time histories of the pitching rate q and yawing rate r can be obtained from equation (A16) as follows:

$$q + ir = R_1 e^{d_H t}\left[(p + \omega_L)\cos(\omega_L t + \nu_1) + \left(d_H + \frac{C_{N_\alpha}}{m'}\right)\sin(\omega_L t + \nu_1)\right]$$

$$+ R_2 e^{d_L t}\left[(p - \omega_H)\cos(\omega_H t - \nu_2) - \left(d_L + \frac{C_{N_\alpha}}{m'}\right)\sin(\omega_H t - \nu_2)\right]$$

$$+ \left(p\beta_{trim} + \frac{C_{N_\alpha}}{m'}\alpha_{trim} - \frac{C_{Z_o}}{m'}\right) + i\left\{R_1 e^{d_H t}\left[(p + \omega_L)\sin(\omega_L t + \nu_1)\right.\right.$$

$$\left. - \left(d_H + \frac{C_{N_\alpha}}{m'}\right)\cos(\omega_L t + \nu_1)\right] + R_2 e^{d_L t}\left[-(p - \omega_H)\sin(\omega_H t - \nu_2)\right.$$

$$\left.\left. - \left(d_L + \frac{C_{N_\alpha}}{m'}\right)\cos(\omega_H t - \nu_2)\right] + \left(p\alpha_{trim} - \frac{C_{N_\alpha}}{m'}\beta_{trim} + \frac{C_{Y_o}}{m'}\right)\right\} \tag{A17}$$

By using fundamental trignometric identities, algebraically collecting terms, and separating the real from the imaginary parts, the following expressions for q and r may be written:

$$r = e^{d_H t}\left\{R_1\left[(p + \omega_L)\cos\nu_1 + \left(d_H + \frac{C_{N_\alpha}}{m'}\right)\sin\nu_1\right]\right\}\sin\omega_L t$$

$$+ e^{d_H t}\left\{R_1\left[(p + \omega_L)\sin\nu_1 - \left(d_H + \frac{C_{N_\alpha}}{m'}\right)\cos\nu_1\right]\right\}\cos\omega_L t$$

(Equation continued on next page)

$$+ e^{d_L t}\left\{R_2\left[-\left(p - \omega_H\right)\cos \nu_2 - \left(d_L + \frac{C_{N_\alpha}}{m'}\right)\sin \nu_2\right]\right\}\sin \omega_H t$$

$$+ e^{d_L t}\left\{R_2\left[\left(p - \omega_H\right)\sin \nu_2 - \left(d_L + \frac{C_{N_\alpha}}{m'}\right)\cos \nu_2\right]\right\}\cos \omega_H t$$

$$+ \left(p\alpha_{trim} - \frac{C_{N_\alpha}}{m'}\beta_{trim} + \frac{C_{Y_o}}{m'}\right) \tag{A18}$$

$$q = e^{d_H t}\left\{R_1\left[-\left(p + \omega_L\right)\sin \nu_1 + \left(d_H + \frac{C_{N_\alpha}}{m'}\right)\cos \nu_1\right]\right\}\sin \omega_L t$$

$$+ e^{d_H t}\left\{R_1\left[\left(p + \omega_L\right)\cos \nu_1 + \left(d_H + \frac{C_{N_\alpha}}{m'}\right)\sin \nu_1\right]\right\}\cos \omega_L t$$

$$+ e^{d_L t}\left\{R_2\left[\left(p - \omega_H\right)\sin \nu_2 - \left(d_L + \frac{C_{N_\alpha}}{m'}\right)\cos \nu_2\right]\right\}\sin \omega_H t$$

$$+ e^{d_L t}\left\{R_2\left[\left(p - \omega_H\right)\cos \nu_2 + \left(d_L + \frac{C_{N_\alpha}}{m'}\right)\sin \nu_2\right]\right\}\cos \omega_H t$$

$$+ \left(p\beta_{trim} + \frac{C_{N_\alpha}}{m'}\alpha_{trim} - \frac{C_{Z_o}}{m'}\right) \tag{A19}$$

where the last terms in parentheses in equations (A18) and (A19) are the r_{trim} and q_{trim} terms, respectively. By simplifying the constant terms, the equations reduce to:

$$r - r_{trim} = e^{d_H t}\left(K_1 \sin \omega_L t + K_2 \cos \omega_L t\right) + e^{d_L t}\left(K_3 \sin \omega_H t + K_4 \cos \omega_H t\right) \tag{A20}$$

$$q - q_{trim} = e^{d_H t}\left(-K_2 \sin \omega_L t + K_1 \cos \omega_L t\right) + e^{d_L t}\left(K_4 \sin \omega_H t - K_3 \cos \omega_H t\right) \tag{A21}$$

Equations (A20) and (A21) are the equations which define the quantities r and q measured by the rate gyros. For the present application the time interval selected for each analysis was less than 1 second of flight time; thus, for these short time intervals

$$e^{d_H t} \approx e^{d_L t} \approx 1$$

Also, examination of the basic data did not clearly indicate any significant effect, if any, of trim on the rates, and therefore, the q_{trim} and r_{trim} terms were neglected. Equations (A20) and (A21) then reduce to the form used in the curve-fit program (eqs. (1) and (2)), namely:

$$r = K_1 \sin \omega_L t + K_2 \cos \omega_L t + K_3 \sin \omega_H t + K_4 \cos \omega_H t$$

$$q = -K_2 \sin \omega_L t + K_1 \cos \omega_L t + K_4 \sin \omega_H t - K_3 \cos \omega_H t$$

Also, equation (A12) may be reduced to:

$$\omega_o = \sqrt{\omega_n^2 + \left(\frac{pI_X}{2I}\right)^2} \tag{A22}$$

where

$$\omega_n^2 = \frac{-C_{m_\alpha} \bar{q} S d}{I} \tag{A23}$$

and

$$\left(\frac{C_{N_\alpha}}{m'} + \frac{C_{m_q}}{I'}\right) \approx 0$$

Simulation Initial Conditions

Given q_o, r_o, $\dot{q}_o$, $\dot{r}_o$, ω_L, and ω_H at an arbitrary starting time within the data interval from the curve-fit program, the remaining initial conditions necessary to start an exact solution using a six-degree-of-freedom computer program to be determined are: the dynamic pressure $\bar{q}_o$, the roll rate p_o, the aerodynamic phase angle φ'_o, the total angle of attack η_o, and the body attitude angles θ_o, ψ_o, and φ_o. The initial dynamic pressure is determined by combining equations (A9), (A10), (A22), and (A23) to yield

$$\bar{q}_o = \frac{I}{-C_{m_\alpha} Sd}\left[\left(\frac{\omega_H + \omega_L}{2}\right)^2 - \left(p_o \frac{I_X}{2I}\right)^2\right] \tag{A24}$$

where the roll rate p_o is determined by solving equations (A9), (A10), and (A14) to give:

$$p_o = \frac{\omega_H - \omega_L}{2\left(1 - \frac{I_X}{2I}\right)} \tag{A25}$$

When equations (A3) and (A4) are modified to permit the use of nonlinear aerodynamics, the initial aerodynamic phase angle φ'_o, the orientation angle of the plane of the velocity vector with respect to the body-axis system, may be determined in the following manner:

$$\dot{r}I + pq\left(I - I_X\right) = \Sigma M_Z = -C_m \sin \varphi' \bar{q} Sd \tag{A26}$$

$$\dot{q}I - pr\left(I - I_X\right) = \Sigma M_Y = C_m \cos \varphi' \bar{q} Sd \tag{A27}$$

Dividing equation (A26) by equation (A27) yields

$$\varphi'_o = \tan^{-1}\left\{\frac{-\left[\dot{r}I + pq\left(I - I_X\right)\right]}{\dot{q}I - pr\left(I - I_X\right)}\right\}_o \tag{A28}$$

Since C_{m_α} is essentially constant up to an angle of attack of approximately 35^o, the initial total angle of attack may now be obtained from

$$\eta_o = \frac{C_{m,o}}{C_{m_\alpha}} \tag{A29}$$

where

$$C_{m,o} = \left(\frac{M_Z}{-\sin \varphi' \bar{q} Sd}\right)_o = \left(\frac{M_Y}{\cos \varphi' \bar{q} Sd}\right)_o \tag{A30}$$

Finally, the body attitude referred to the gravity-axis system (fig. 6) is determined with the assumption that the initial roll position φ_o may be arbitrarily selected since it has little effect, if any, on the relative motion patterns of the body and affects only the orientation of the inertial motion patterns. The body pitch and yaw angles θ and ψ, respectively, may now be obtained by trigonometrically adding η_o and φ'_o to the pitch and

yaw flight-path angles γ_p and γ_y, respectively, from the trajectory to yield:

$$\theta_o = \sin^{-1}\left(\frac{\sin\gamma_p \cos\eta + \sin\eta\cos\varphi_G\sqrt{\cos^2\eta + \sin^2\eta\cos^2\varphi_G - \sin^2\gamma_p}}{\cos^2\eta + \sin^2\eta\cos^2\varphi_G}\right)_o \tag{A31}$$

and

$$\psi_o = \gamma_{y,o} - \sin^{-1}\left(\frac{\sin\eta\sin\varphi_G}{\cos\gamma_p}\right)_o \tag{A32}$$

where

$$\varphi_{G,o} = \left(\varphi' - \varphi\right)_o \tag{A33}$$

APPENDIX B

EQUATIONS OF MOTION USED IN THE SIX-DEGREE-OF-FREEDOM COMPUTER PROGRAM

The equations used in the simulations of this analysis may be found in reference 9, with the exception that the trajectory calculations were made with respect to an oblate spheroidal earth rather than the spherical earth of reference 9. These equations are a part of a general computer program which is described in detail in reference 6. Only the equations directly related to the simulation of rate and accelerometer data and to the generation of corresponding relative and inertial motion patterns are presented herein. To simulate the accelerometer data of instruments located off the center of gravity, the accelerometer transfer equations from reference 10 were added to those of the general computer program. The motion equations of the program are written for a rigid body with variable mass and determine both the translatory and rotational motions of the center of gravity of the body in three-dimensional space. The Standard Atmosphere, 1962 (ref. 7), was programed. Unlike the curve-fit program of appendix A, there were no restrictions on free-stream conditions, gravitational forces were considered, and allowance was made for large angles and nonlinear aerodynamics. Roll rate, however, was held constant within each interval, although it was permitted to change from one data period to another. The forces and moments due to damping, Magnus effects, and aerodynamic and mass asymmetries were neglected. With the preceding conditions, the equations were reduced to the following:

$$m(\dot{u} + wq - vr) + mg \sin \theta = mgA_{X,cg} = C_X \bar{q} S \tag{B1}$$

$$m(\dot{v} + ur - wp) - mg \cos \theta \sin \varphi = mgA_{Y,cg} = -C_R \sin \varphi' \bar{q} S \tag{B2}$$

$$m(\dot{w} + vp - uq) - mg \cos \theta \cos \varphi = mgA_{Z,cg} = -C_R \cos \varphi' \bar{q} S \tag{B3}$$

$$\dot{p} I_X = 0 \tag{B4}$$

$$\dot{q} I - pr(I - I_X) = C_m \cos \varphi' \bar{q} S d \tag{B5}$$

$$\dot{r} I + pq(I - I_X) = -C_m \sin \varphi' \bar{q} S d \tag{B6}$$

APPENDIX B

The earth-relative velocity $\overline{V}$, was calculated by vectorially subtracting the rotational velocity of the earth from the inertial velocity of the body. The angles of attack and yaw of the vehicle were computed in terms of $\overline{V}$ and its components along the body axis, $\overline{u}$, $\overline{v}$, and $\overline{w}$, as follows:

$$\alpha = \tan^{-1} \frac{\overline{w}}{\overline{u}} \tag{B7}$$

$$\beta = \sin^{-1} \frac{\overline{v}}{\overline{V}} \tag{B8}$$

The total angle of attack and its phase angle may be defined in terms of the components angles, α and β, as follows

$$\eta = \cos^{-1}(\cos \alpha \cos \beta) \tag{B9}$$

$$\varphi' = \tan^{-1} \frac{\tan \beta}{\sin \alpha} \tag{B10}$$

The trajectory equations of the program are the usual three-dimensional expressions and are not repeated here.

The attitude of the vehicle with respect to the gravity-axis system is defined by Euler angles (see fig. 6) and are calculated from the following equations:

$$\theta = \theta_o + \int \left(q \cos \varphi - r \sin \varphi - K_\theta\right) dt \tag{B11}$$

$$\psi = \psi_o + \int \left(\frac{r \cos \varphi + q \sin \varphi}{\cos \theta} + K_\psi\right) dt \tag{B12}$$

$$\varphi = \varphi_o + \int \left(p + \dot{\psi} \sin \theta + K_\varphi\right) dt \tag{B13}$$

where K_θ, K_ψ, and K_φ are the body-axis components of the angular velocity of the local gravity-axis system moving with the vehicle with respect to an inertial reference. (See ref. 9.)

Finally, the equations for determining the off-center-of-gravity accelerations (ref. 10) were obtained from:

$$A_{X,i} = A_{X,cg} - \frac{1}{g}\left[x_X\left(q^2 + r^2\right) + y_X(\dot{r} - pq) - z_X(\dot{q} + rp)\right] \tag{B14}$$

$$A_{Y,i} = A_{Y,cg} - \frac{1}{g}\left[-x_y(\dot{r} + pq) + y_y\left(r^2 + p^2\right) + z_y(\dot{p} - qr)\right] \tag{B15}$$

$$A_{Z,i} = A_{Z,cg} - \frac{1}{g}\left[x_z(\dot{q} - rp) - y_z(\dot{p} + qr) + z_z\left(p^2 + q^2\right)\right] \tag{B16}$$

REFERENCES

1. Dingeldein, Richard C.: Flight Measurements of Reentry Heating at Hyperbolic Velocity (Project Fire). NASA TM X-1053, 1965.

2. Scallion, William I.; and Lewis, John H., Jr.: Flight Parameters and Vehicle Performance for Project Fire Flight 1 Launched April 14, 1964. NASA TN D-2996, 1965.

3. SLV Test Evaluation and Guidance Software Groups: Project Fire Integrated Post Flight Evaluation Report – Flight No. 1. GDA/BKF-64-018 (NASA CR-57017), Gen. Dyn./Astronaut., Oct. 30, 1964.

4. Morgan, James R.; and Fournier, Roger H.: Static Longitudinal Aerodynamic Characteristics of a 0.07-Scale Model of a Proposed Apollo Spacecraft at Mach Numbers of 1.57 to 4.65. NASA TM X-603, 1961.

5. Nelson, Robert L.: The Motions of Rolling Symmetrical Missiles Referred to a Body-Axis System. NACA TN 3737, 1956.

6. Dennison, A. J.; and Butler, J. F.: Missile and Satellite Systems Program for the I.B.M. 7090. Tech. Inform. Ser. No. 61 SD 170, Missile and Space Vehicle Dept., Gen. Elec. Co., Feb. 1962.

7. Anon.: U.S. Standard Atmosphere, 1962. NASA, U.S. Air Force, and U.S. Weather Bur., Dec. 1962.

8. Cauchon, Dona L.: Project Fire Flight 1 Radiative Heating Experiment. NASA TM X-1222, 1966.

9. Mayhue, Robert J.: Determination of Trajectory and Angles of Attack of a Scout Heat-Transfer Spacecraft During Reentry Flight in the Atmosphere. NASA TN D-2776, 1965.

10. Lovelace, Uriel M.; Hoffman, Sherwood; and Mayhue, Robert J.: Analysis of the Trajectory and Large-Amplitude Motions of a Scout Vehicle During Fourth-Stage Reentry Flight. NASA TN D-2309, 1964.

TABLE 1.- SEQUENCE OF EVENTS DURING REENTRY

Event	Elapsed flight time, t, sec
Reentry-package separation	1640.5
Reentry commences (h = 121 920 m)	1647.4
Begin telemeter blackout	1653.9
Begin C-band radar blackout	1660.2
Disturbance	1665.94
First heat-shield ejection (signal)	1669.6
Second heat-shield ejection (signal)	1676.6
End telemeter blackout	1686.8
Reentry-package impact	1965.7

TABLE 2.- MOTION-INSTRUMENTATION RANGES

PLUS ACCELEROMETER LOCATIONS

Motion instrument	Range	Location		
		x, m (Fire sta.)	y_b, m	z_b, m
Axial accelerometer, A_X	0 to -120g	0.4550	0.0475	-0.0393
Transverse accelerometer, A_Y	+6g to -6g	.5105	0	-.0315
Normal accelerometer, A_Z	+6g to -6g	.5105	.0546	0
Roll-rate gyro, p	0 to 35 radians/sec			
Pitch-rate gyro, q	±3 radians/sec			
Yaw-rate gyro, r	±3 radians/sec			

TABLE 3.- SUMMARY OF INPUT AND RESULTS OF CURVE-FIT PROGRAM FOR SEVEN DATA INTERVALS

Date period . . .	I	II	III	IV	V	VI	VII
Time interval,	1667.64	1670.36	1673.06	1676.21	1679.61	1683.17	1686.85
sec	1668.38	1671.08	1673.84	1676.95	1680.38	1683.91	1687.68
t_1	1667.64	1670.36	1673.06	1676.21	1679.61	1683.17	1686.85
t_2	1667.70	1670.40	1673.08	1676.23	1679.63	1683.22	1686.92
t_3	1667.92	1670.62	1673.26	1676.30	1679.67	1683.26	1686.99
t_4	1668.05	1670.65	1673.28	1676.32	1679.71	1683.32	1687.05
$^*\Delta t_1$	0	0	0	0	0	0	0
Δt_2	.06	.04	.02	.02	.02	.05	.07
Δt_3	.28	.26	.20	.09	.06	.09	.14
Δt_4	.41	.29	.22	.11	.10	.15	.20
$^\dagger r_1$	-2.793	-2.863	1.116	2.874	2.862	-2.974	-2.698
r_2	2.915	2.498	-2.175	-2.323	-2.072	.617	1.145
r_3	2.887	1.991	-1.874	-1.911	-2.846	-2.784	-2.690
r_4	-2.649	-2.793	2.666	2.482	.830	2.478	2.989
ω_L	9.6	14.475	22.100	27.700	32.70	27.85	19.03
ω_H	23.74	26.055	35.36	43.300	45.16	40.06	30.72
K_1	6.767	8.318	-4.877	-3.385	-.704	-4.645	-2.021
K_2	-1.279	-5.167	5.486	.625	5.129	-1.947	-2.844
K_3	.528	1.285	-2.656	-3.325	-5.490	5.620	4.614
K_4	-1.514	2.304	-4.370	2.252	-2.267	-1.027	.146

$^*\Delta t_n = t_n - t_1$.

$^\dagger r$ represents yaw rate data points used in eq. (1).

TABLE 4.- SUMMARY OF INITIAL CONDITIONS USED IN EXACT SOLUTION FOR SIMULATION OF SEVEN DATA INTERVALS

Data period	Time interval, sec	p, $\frac{\text{radians}}{\text{sec}}$	r, $\frac{\text{radians}}{\text{sec}}$	q, $\frac{\text{radians}}{\text{sec}}$	$\dot{r}$, $\frac{\text{radians}}{\text{sec}^2}$	$\dot{q}$, $\frac{\text{radians}}{\text{sec}^2}$	$\overline{V}$, m/sec	h, m	γ_p, deg	$\overline{q}$, N/m^2	φ', deg	η, deg	α, deg	β, deg	φ, deg	θ, deg	ψ, deg	C_{m_α}
I	1667.64 to 1668.38	18.85	-2.793	6.240	77.536	-23.698	11 430	63 330	-13.06	13 344	52.552	24.954	15.798	19.569	0	1.922	101.889	-0.1175
II	1670.36 to 1671.08	14.80	-2.863	7.034	153.865	134.816	11 130	56 529	-12.56	28 924	133.744	32.273	-23.589	22.690	0	-37.222	98.681	-.1265
III	1673.06 to 1673.84	16.935	1.116	-2.222	-201.322	-275.208	10 488	49 116	-12.30	63 030	324.531	26.570	22.161	-15.043	0	9.418	137.295	-.1269
IV	1676.21 to 1676.95	19.75	2.874	-.06	-237.768	80.236	8 831	43 434	-11.120	95 349	248.783	12.882	-4.731	-11.995	0	-16.103	134.068	-.1320
V	1679.61 to 1680.38	15.22	2.862	4.786	-245.877	-271.890	6 756	38 401	-10.900	115 367	315.55	14.500	10.460	-10.098	0	-.614	132.086	-.1360
VI	1683.17 to 1683.91	14.92	-2.974	-10.265	100.531	13.258	4 538	35 006	-10.100	87 085	92.315	6.410	-.260	6.405	0	-10.424	115.274	-.1380
VII	1686.85 to 1687.68	14.30	-2.698	-6.632	106.890	59.965	2 797	33 071	-8.100	44 768	113.100	13.450	-5.360	12.354	0	-13.654	109.330	-.1380

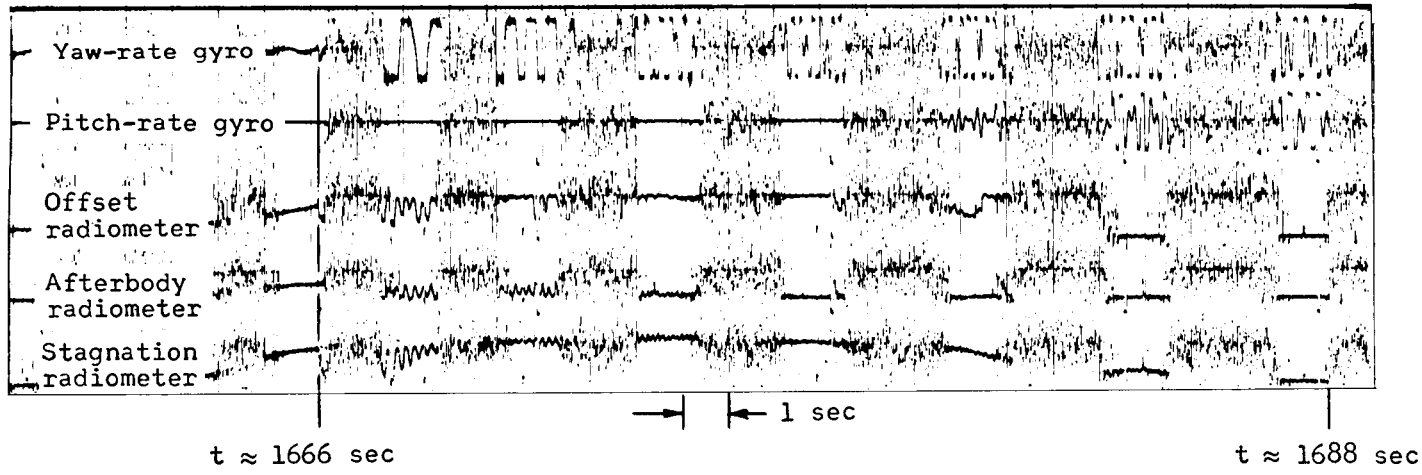

(a) First playback.

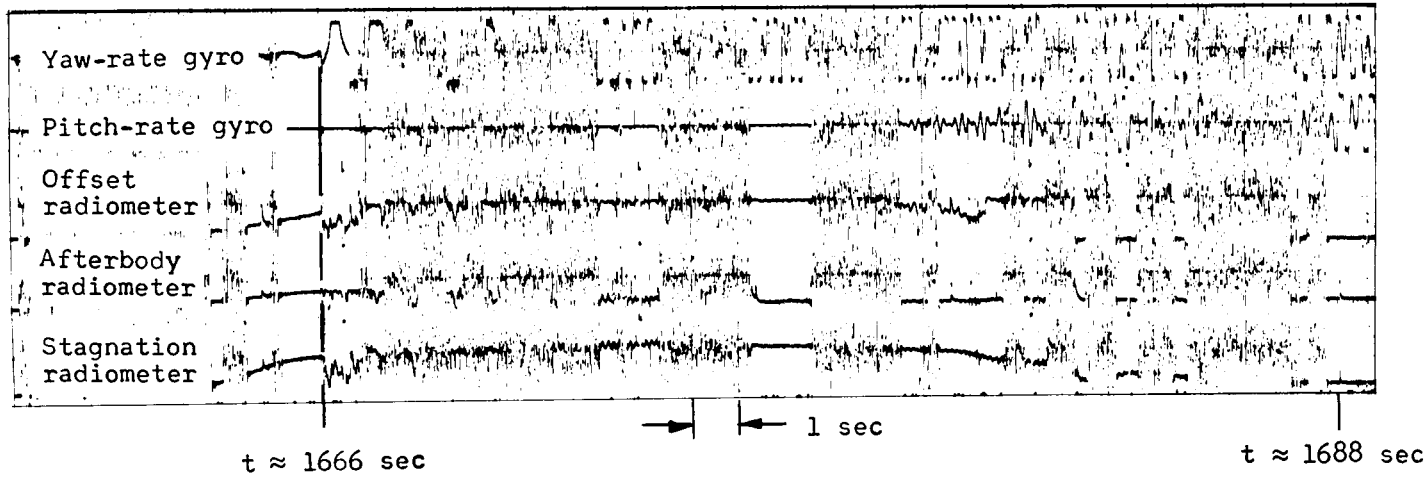

(b) Second playback.

Figure 1.- Photographs of first and second playbacks of telemetered data.

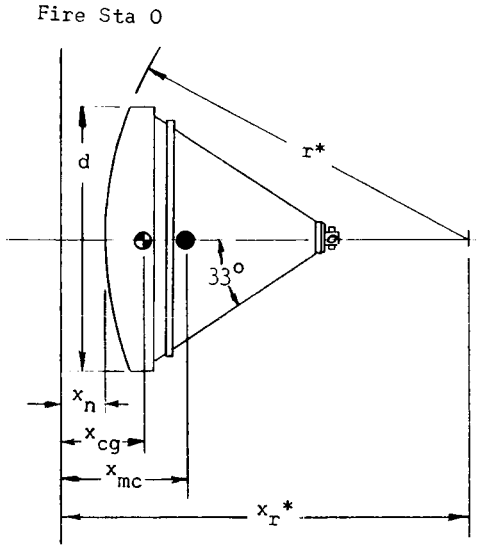

$x_n^* = x_r^* - r^*$

$x_{mc}^* = x_n^* + .2875\ d$

(a) Sketch of Project Fire payload.

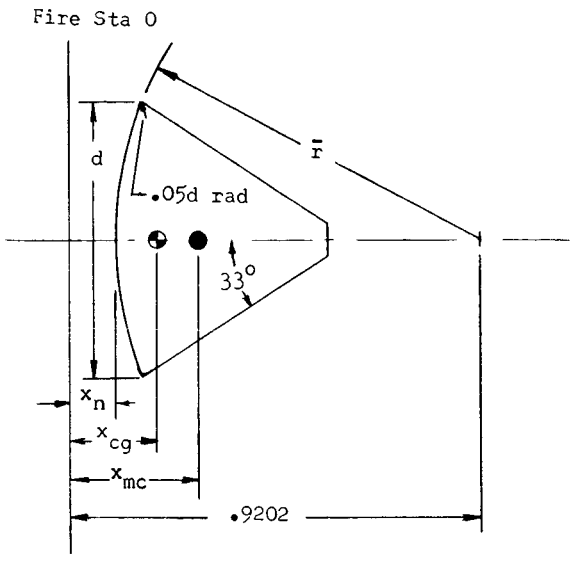

$\bar{r} = 1.2\ d$

$x_n = .9202 - \bar{r}$

$x_{mc} = x_n + .2875\ d$

(b) Sketch of wind-tunnel model.

Configuration / Time Group	m	x_{cg}	I_X	I	d	r*	x_r*
Complete Reentry Payload 1640.5 to 1667.9 sec	83.28	.2809	3.36	2.687	.6721	.9347	1.0480
Less first calorimeter 1668.7 to 1670.0 sec	79.88	.2863	3.13	2.52	.6543	.9286	1.0480
Less first phenolic layer 1670.001 to 1672.9 sec	72.76	.2974	2.66	2.18	.6299	.8052	.9373
Less second calorimeter 1675.1 to 1676.6 sec	68.90	.3045	2.41	1.99	.6071	.7991	.9373
Less second phenolic layer 1676.601 to 1679.9 sec	62.91	.3150	2.03	1.72	.5870	.7021	.8519
Less third calorimeter 1680.8 to splash	60.87	.3200	1.94	1.64	.5763	.6960	.8519

General dimensions and mass characteristics.

Figure 2.- Physical properties of flight and wind-tunnel models. Linear dimensions are in meters.

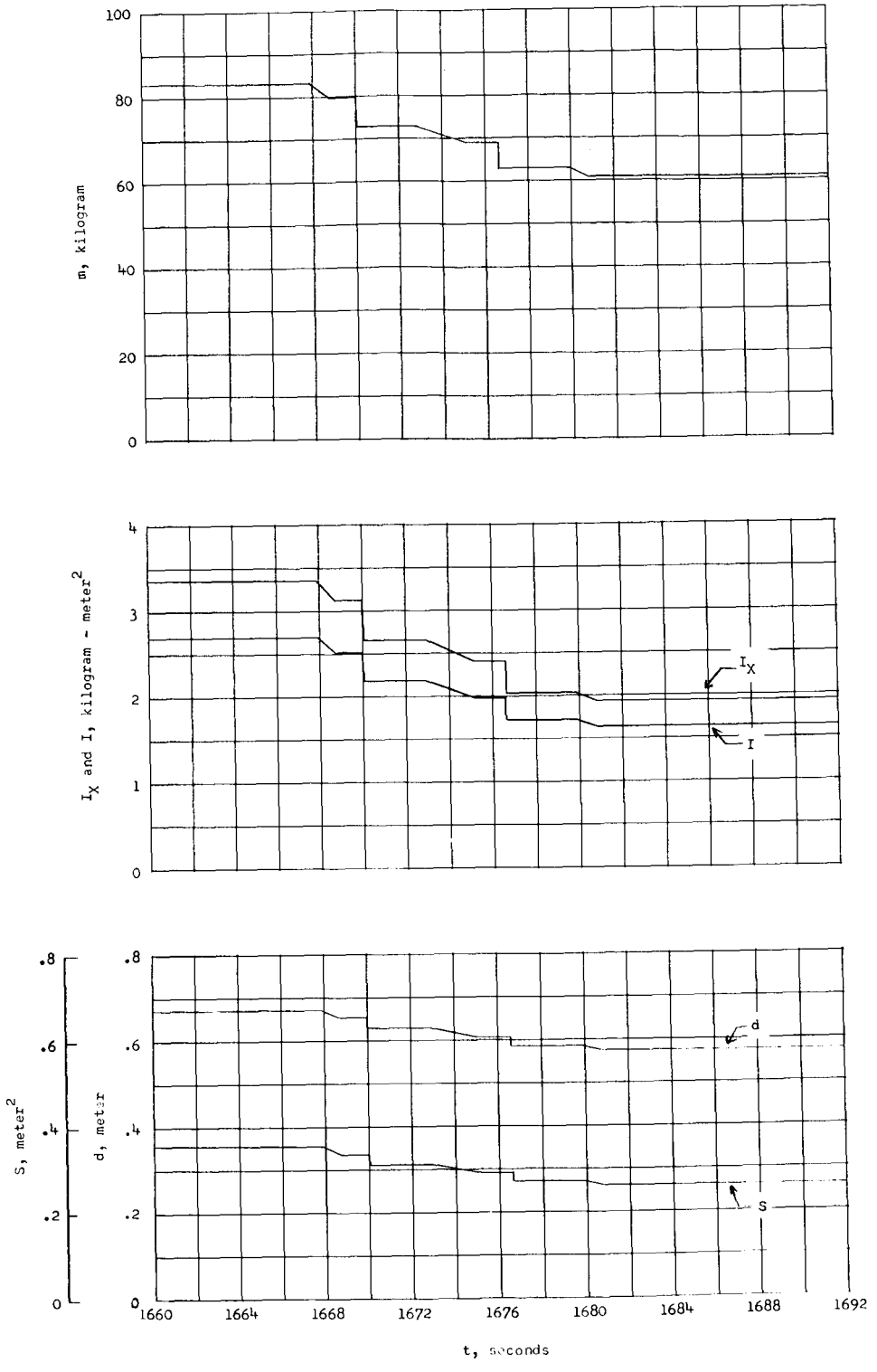

Figure 3.- Variation of m, I_X, I, S, and d with time.

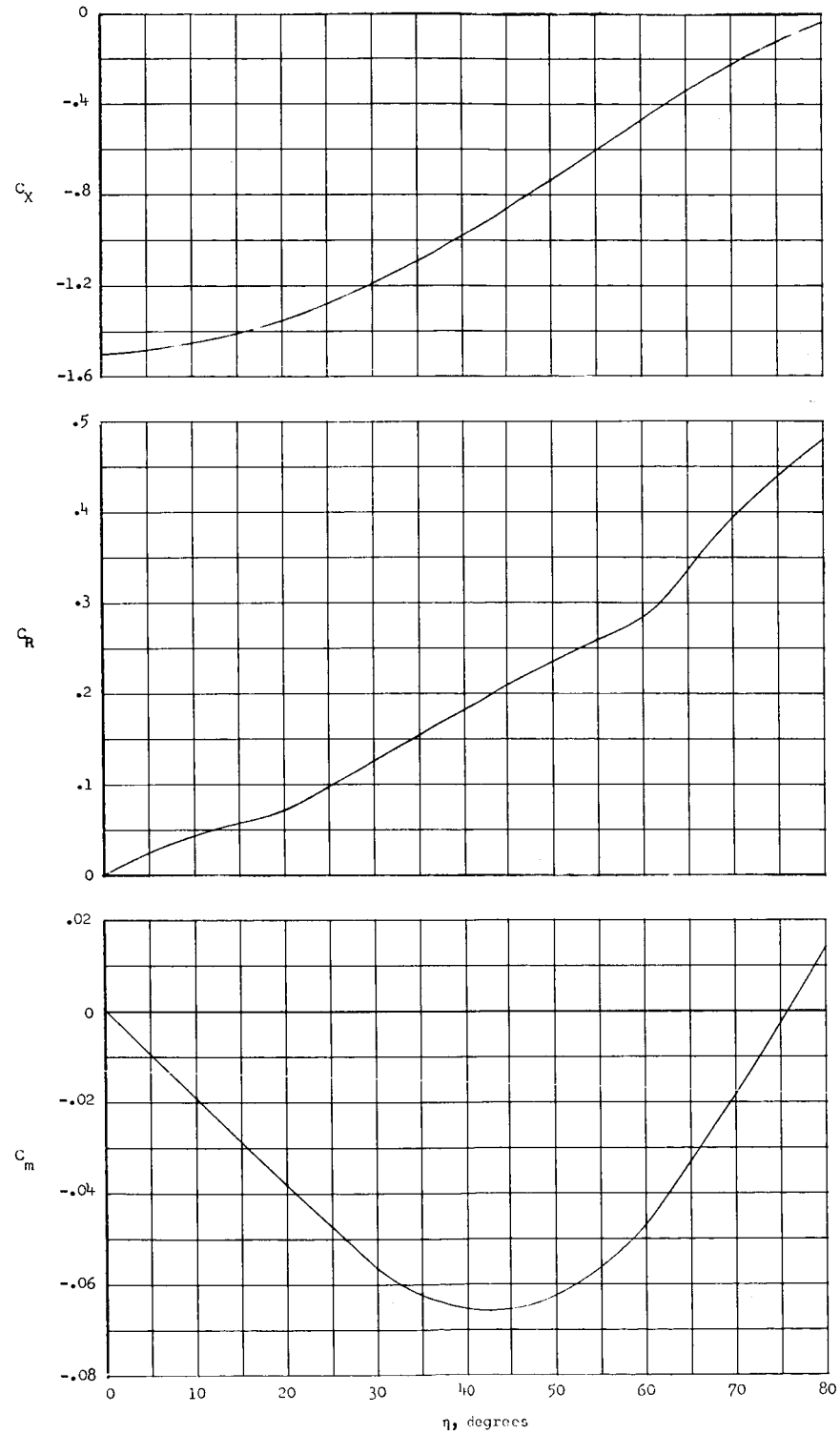

Figure 4.- Wind-tunnel aerodynamic coefficients used in simulations of flight data. Moment center is 0.2875d to rear of face of body.

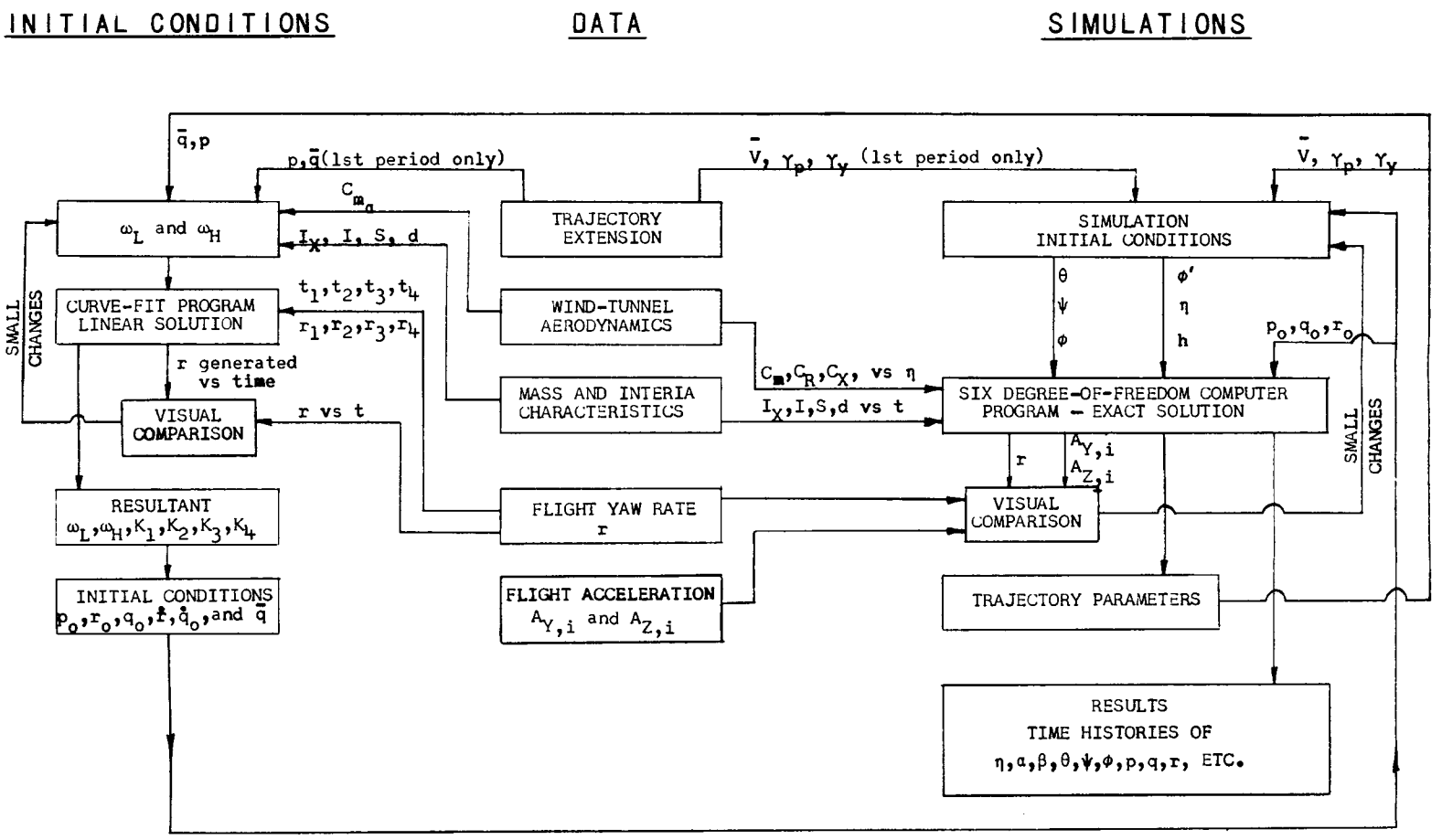

Figure 5.- Block diagram summarizing simulation techniques used in analysis of Fire 1 flight.

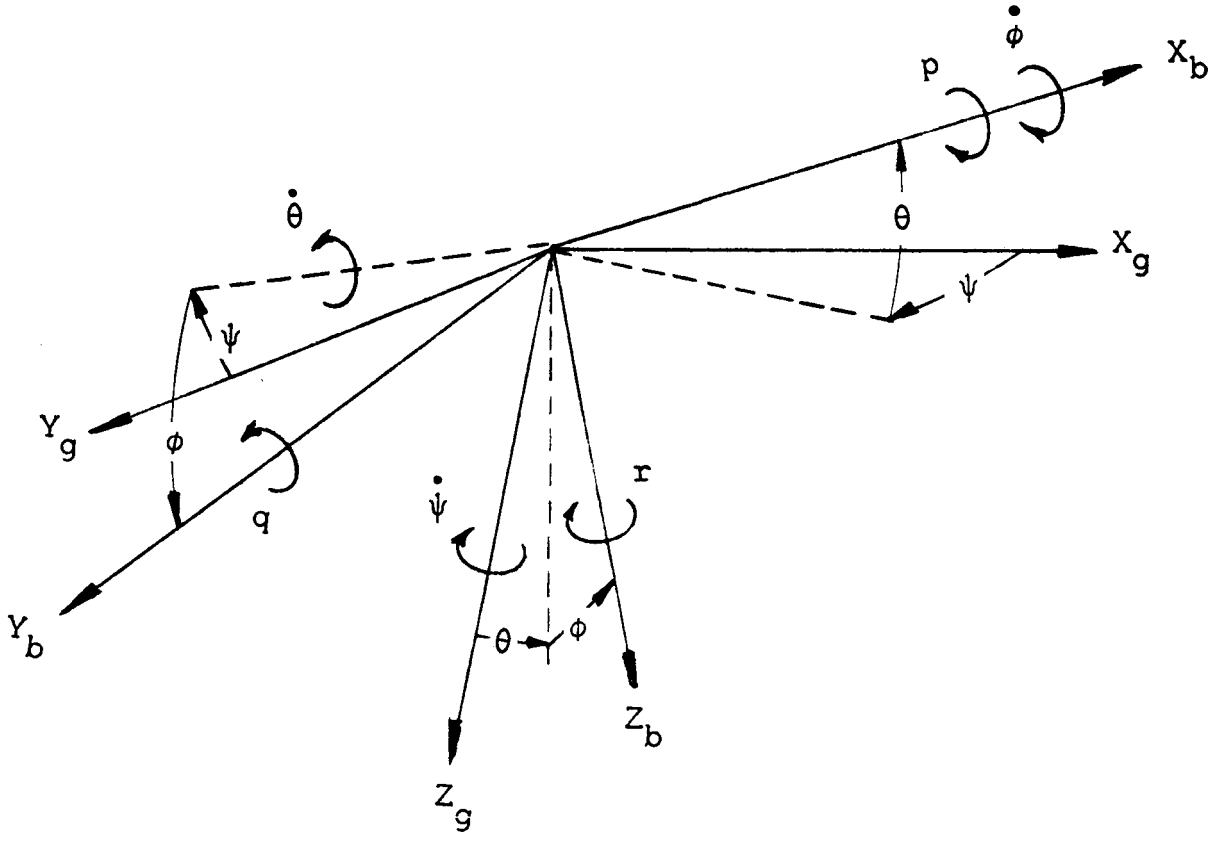

(a) Gravity and body-axis systems.

Figure 6.- Axis systems.

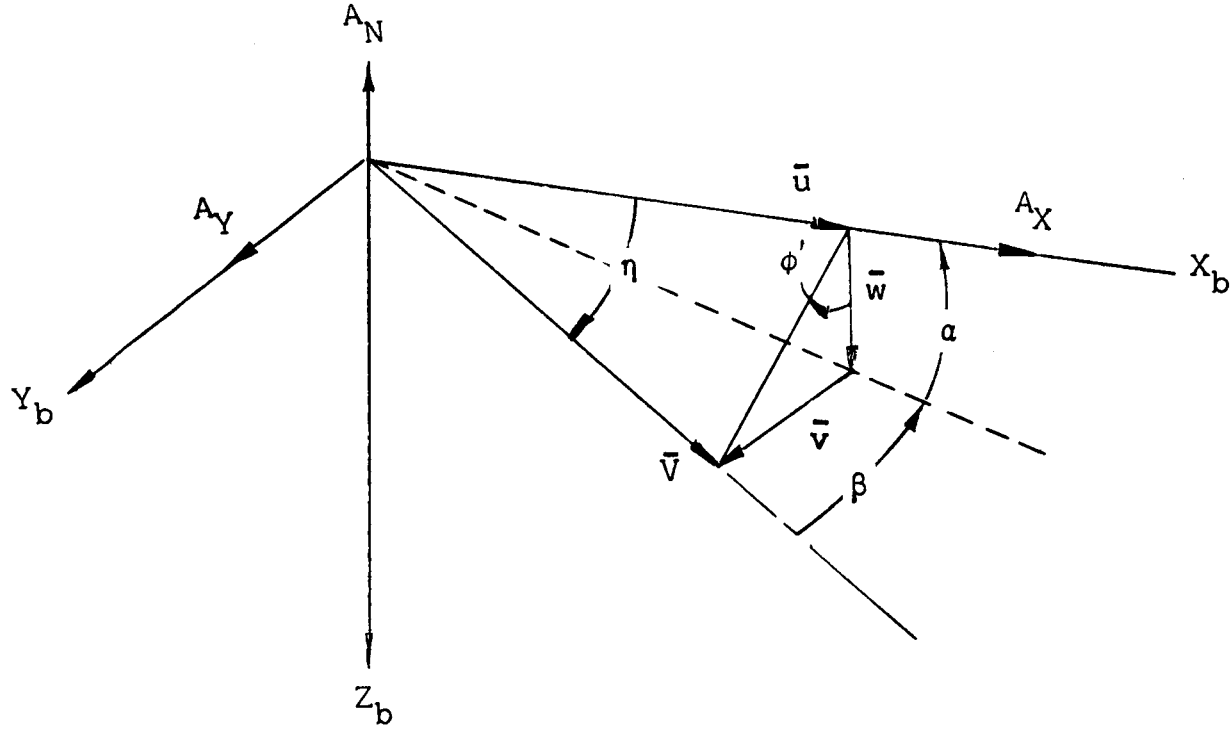

(b) Velocity vector orientation with respect to body-axis system.

Figure 6.- Concluded.

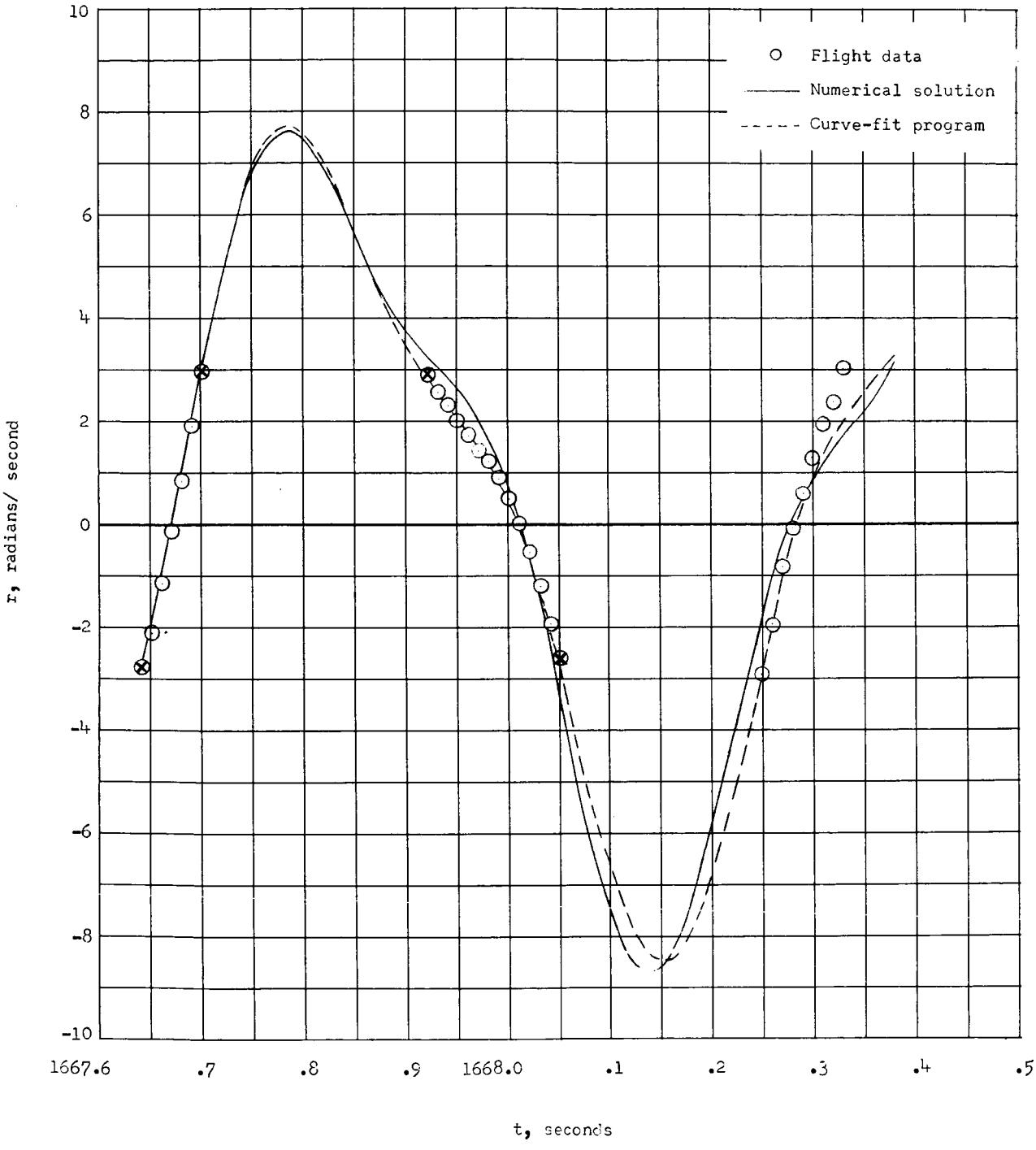

(a) Yaw rates.

Figure 7.- Comparison of computed data with corresponding measured flight data. 1667.64 to 1668.38 seconds. Crossed symbols indicate data points selected for curve-fit program.

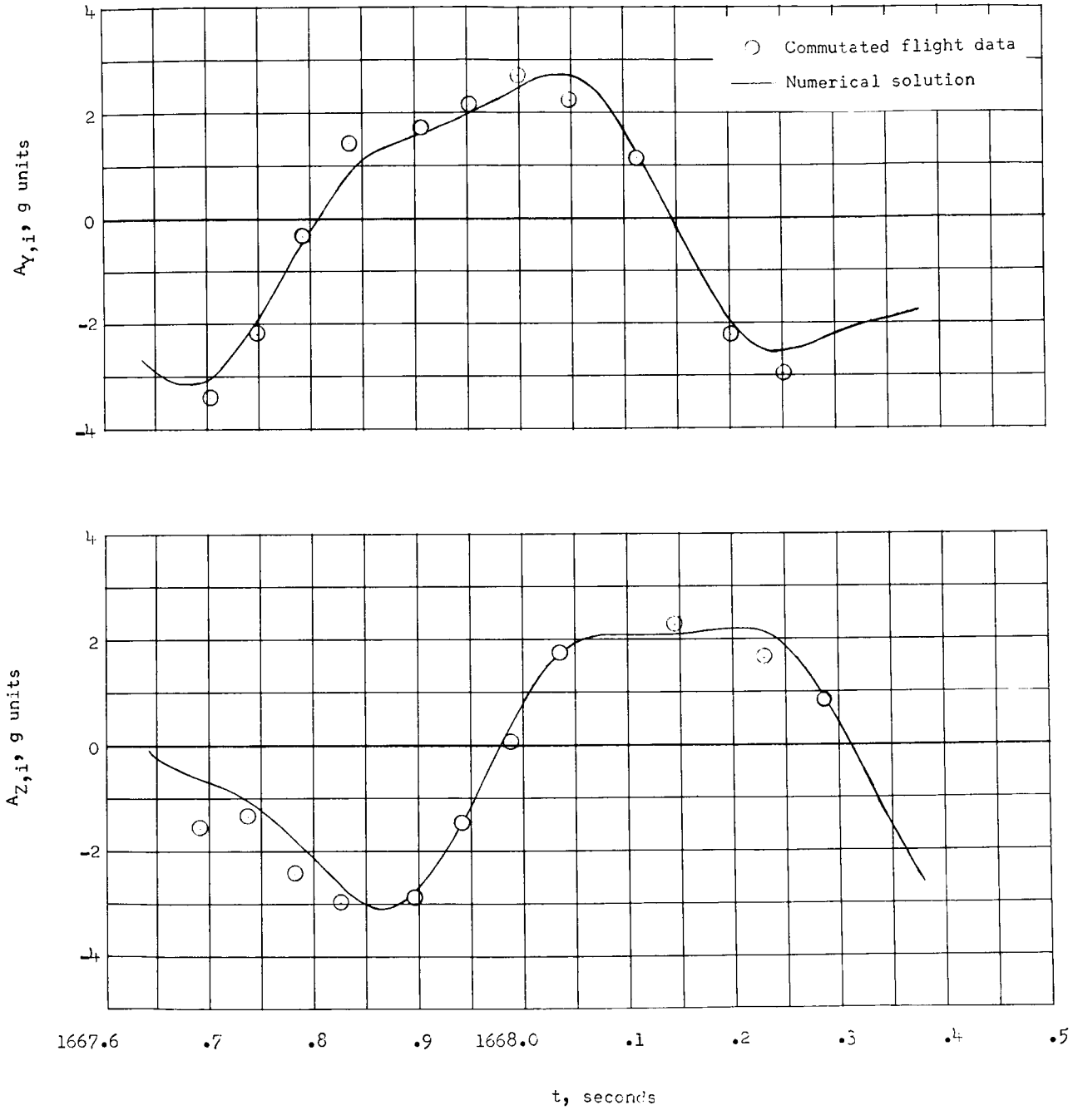

(b) Indicated accelerations.

Figure 7.- Concluded.

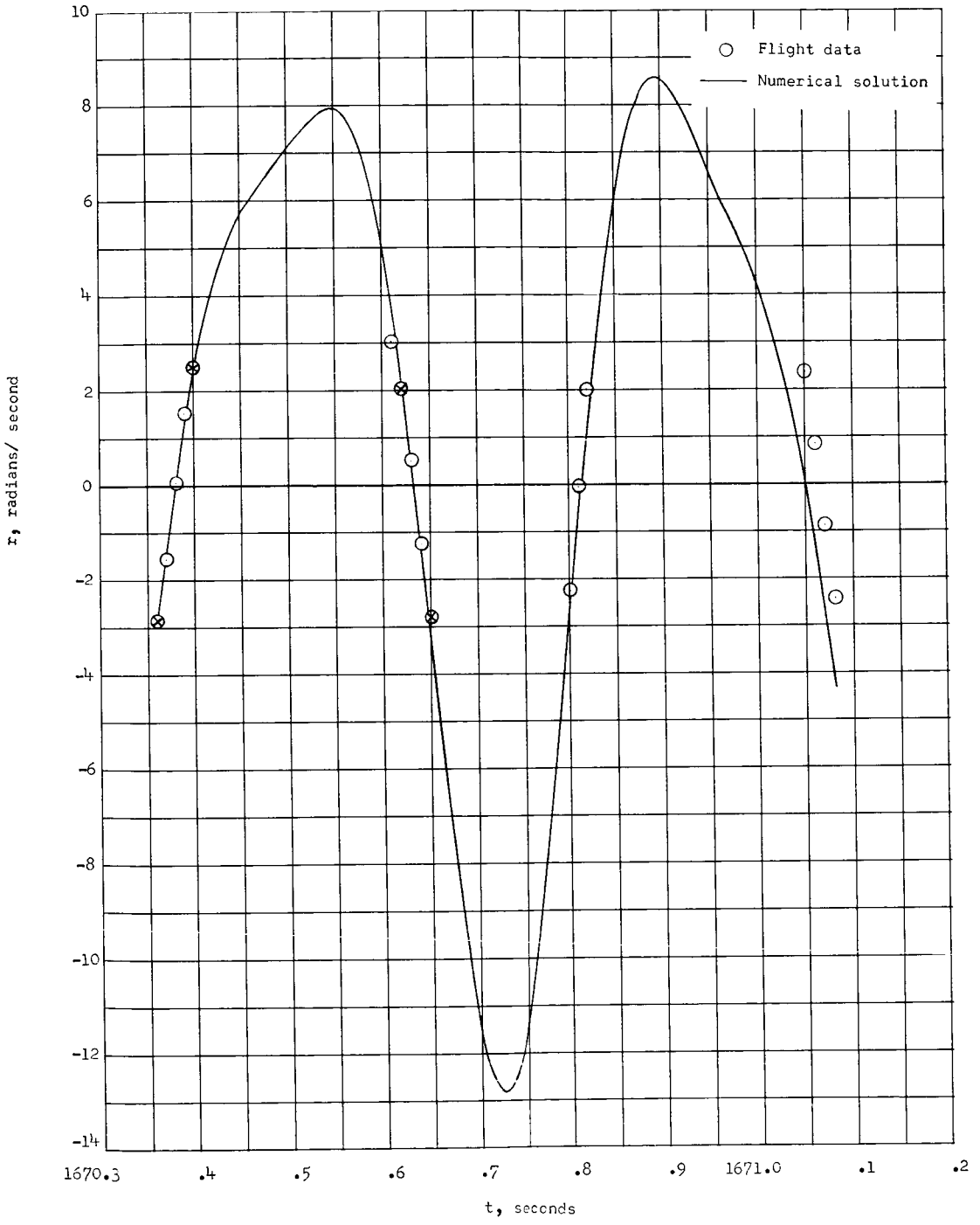

(a) Yaw rates.

Figure 8.- Comparison of computed data with corresponding measured flight data. 1670.36 to 1671.08 seconds. Crossed symbols indicate data points selected for curve-fit program.

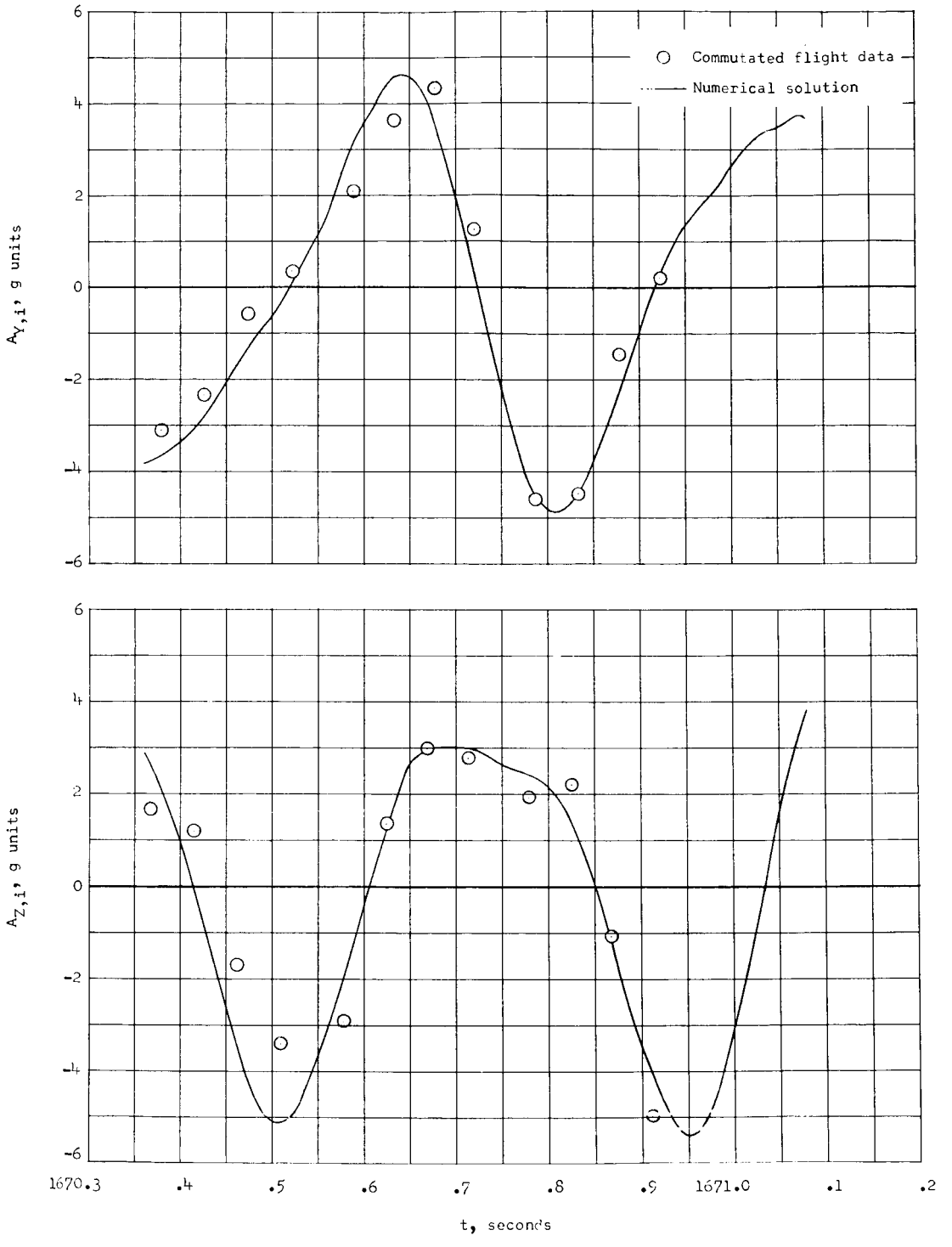

(b) Indicated accelerations.

Figure 8.- Concluded.

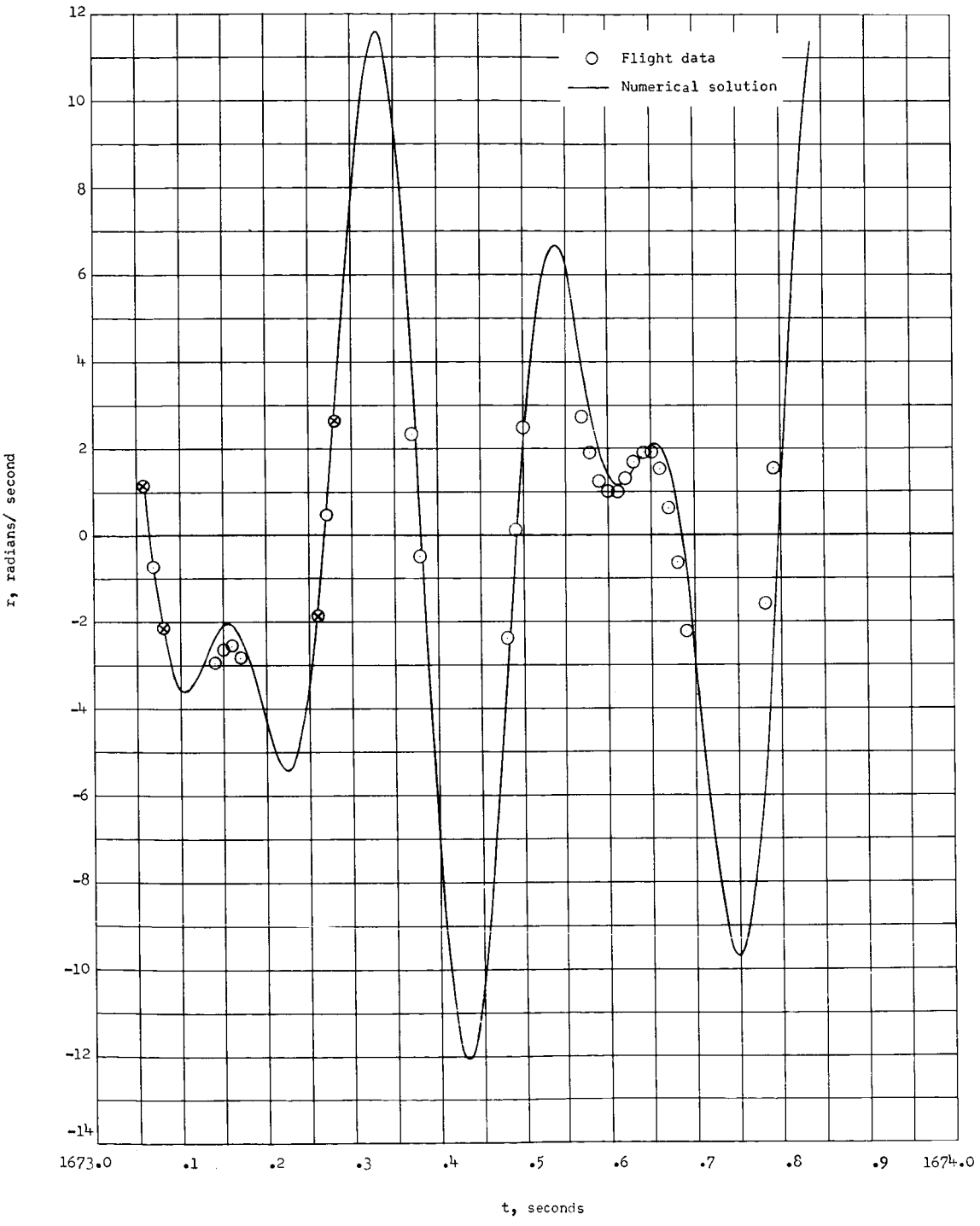

(a) Yaw rates.

Figure 9.- Comparison of computed data with corresponding measured flight data. 1673.06 to 1673.84 seconds. Crossed symbols indicate data points selected for curve-fit program.

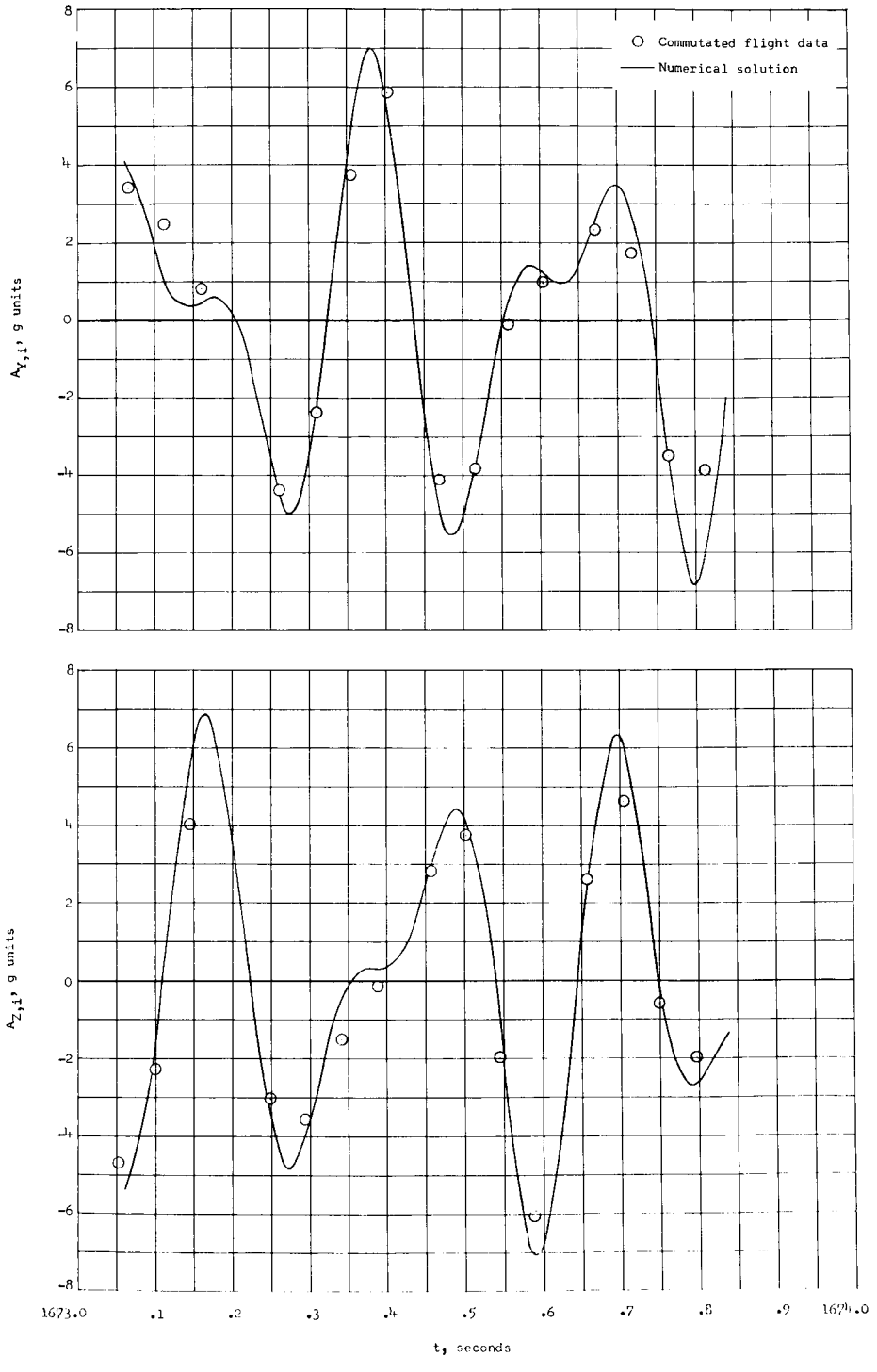

(b) Indicated accelerations.

Figure 9.- Concluded.

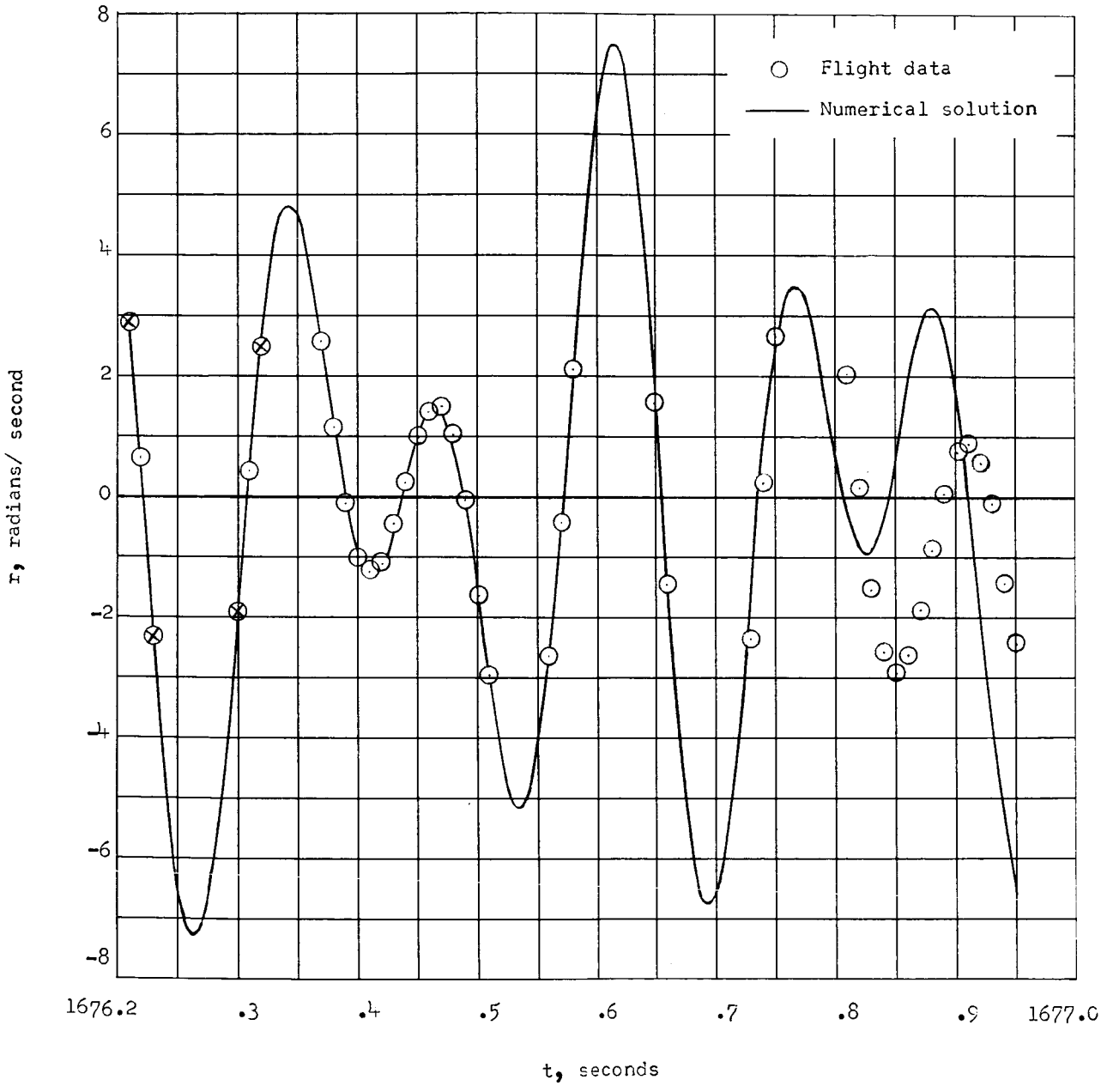

(a) Yaw rates.

Figure 10.- Comparison of computed data with corresponding measured flight data. 1676.21 to 1676.95 seconds. Crossed symbols indicate data points selected for curve-fit program. Flagged symbols represent data from a different playback.

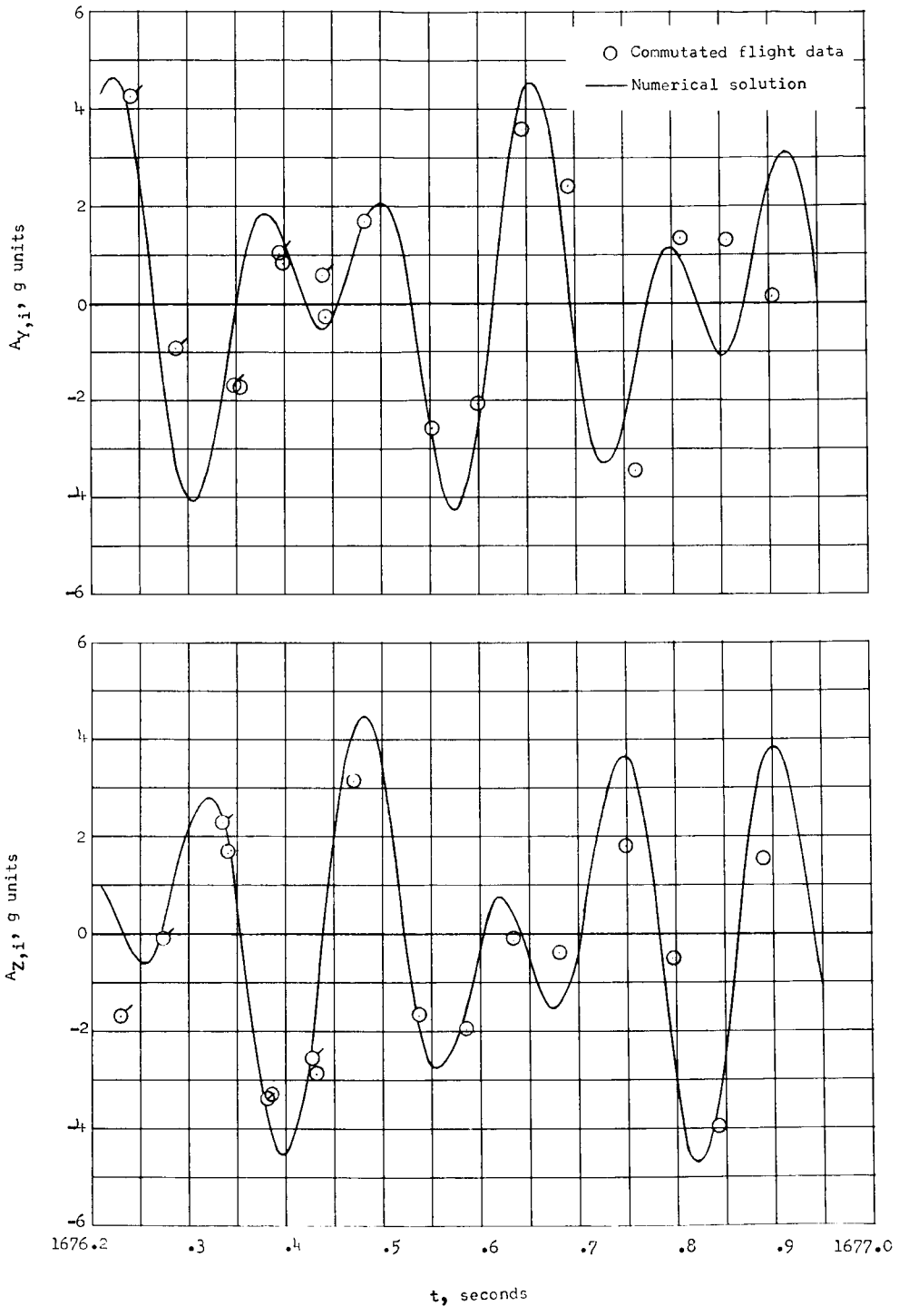

(b) Indicated accelerations.

Figure 10.- Concluded.

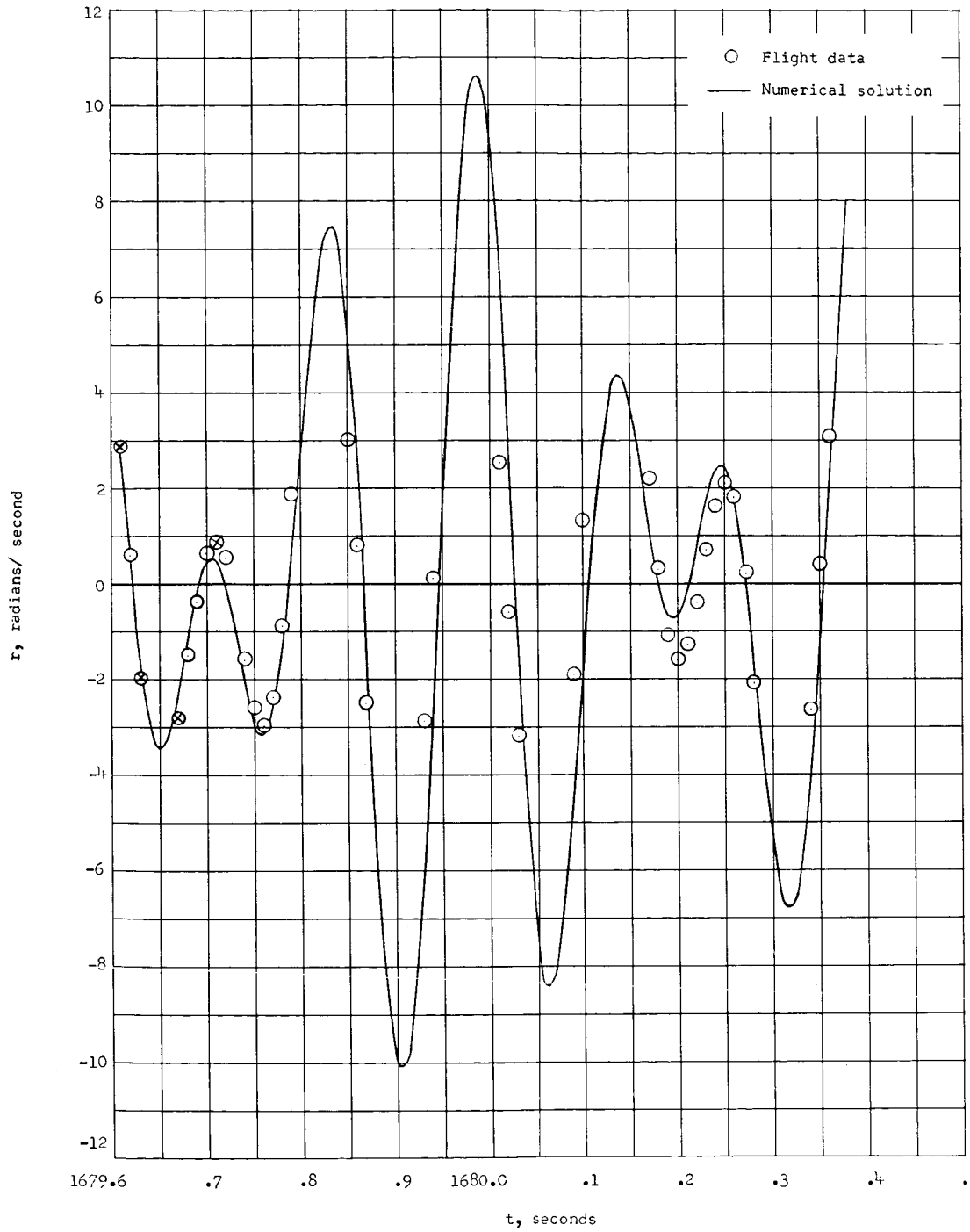

(a) Yaw rates.

Figure 11.- Comparison of computed data with corresponding measured flight data. 1679.61 to 1680.37 seconds. Crossed symbols represent data points selected for curve-fit program. Flagged symbols represent data from a different playback.

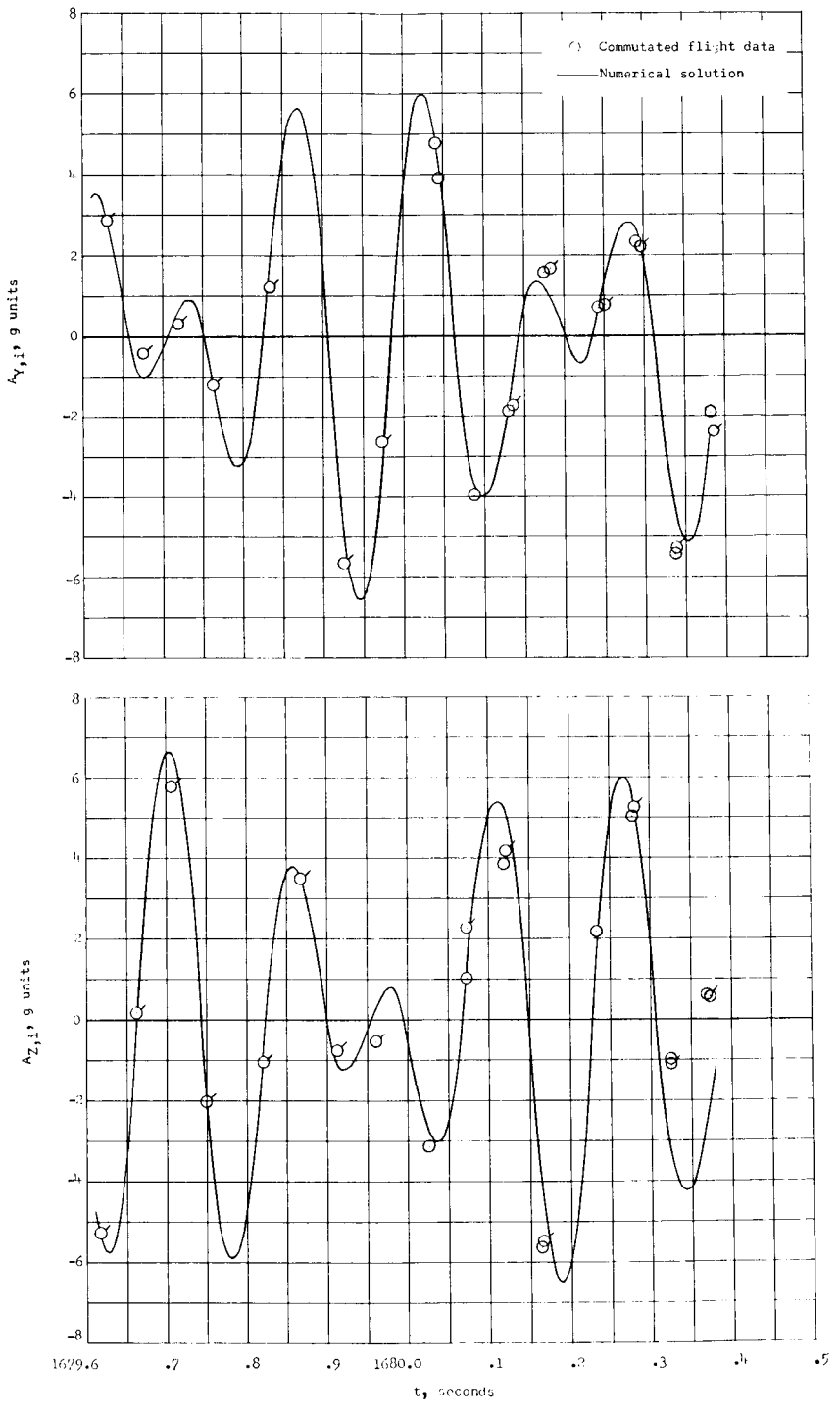

(b) Indicated accelerations.

Figure 11.- Concluded.

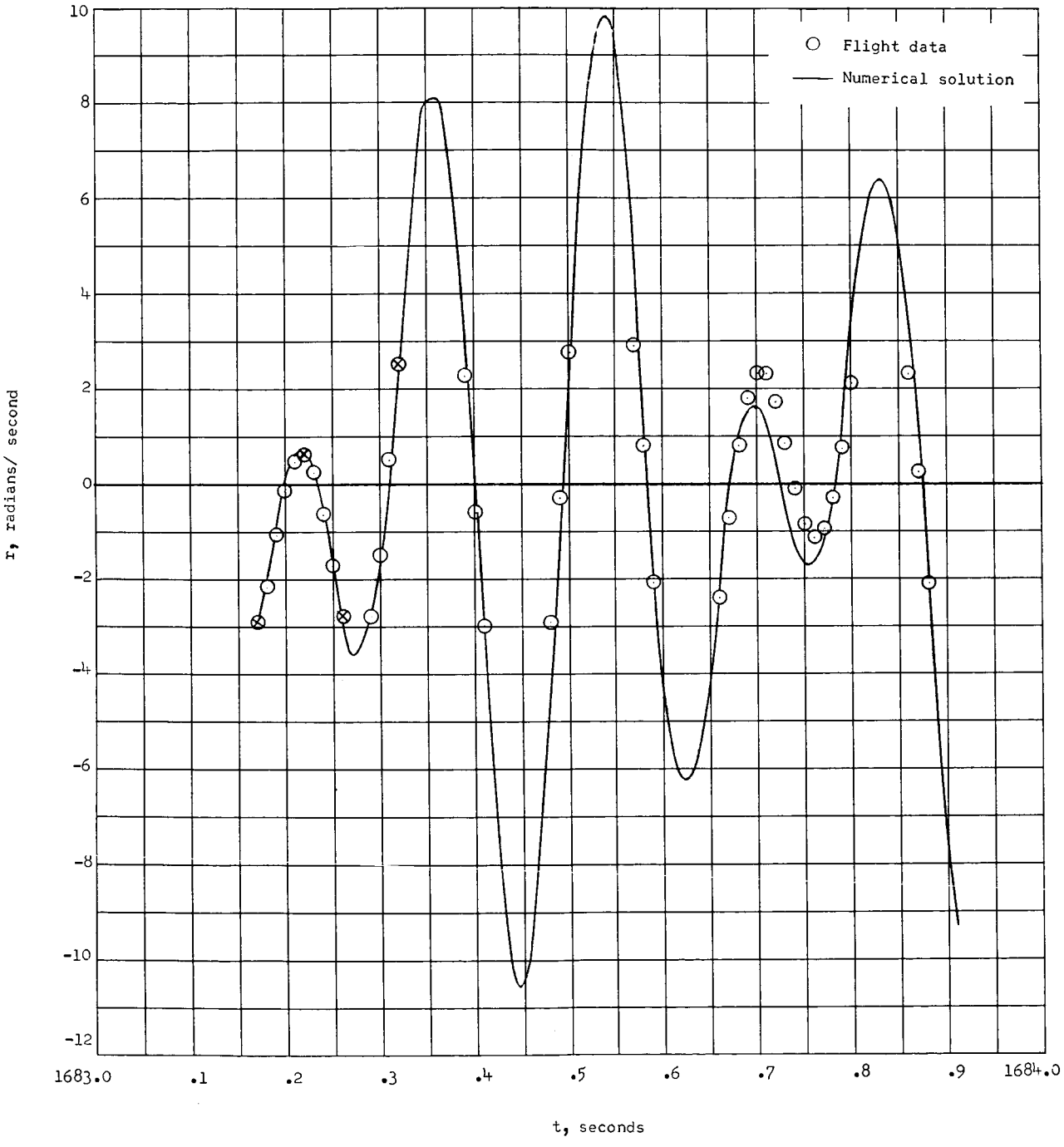

(a) Yaw rates.

Figure 12.- Comparison of computed data with corresponding measured flight data. 1683.17 to 1683.91 seconds. Crossed symbols represent data points selected for curve-fit program. Flagged symbols represent data from a different playback.

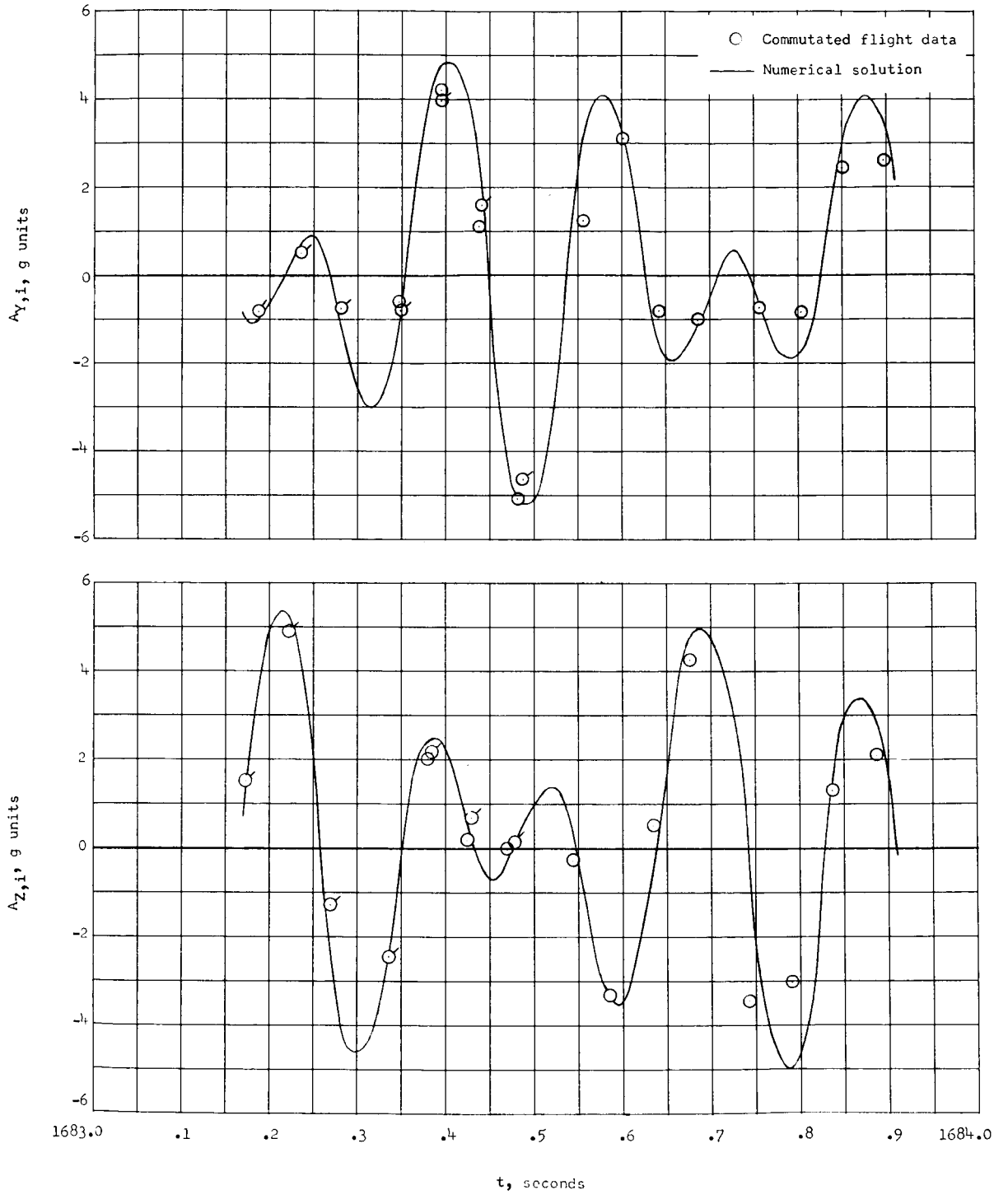

(b) Indicated accelerations.

Figure 12.- Concluded.

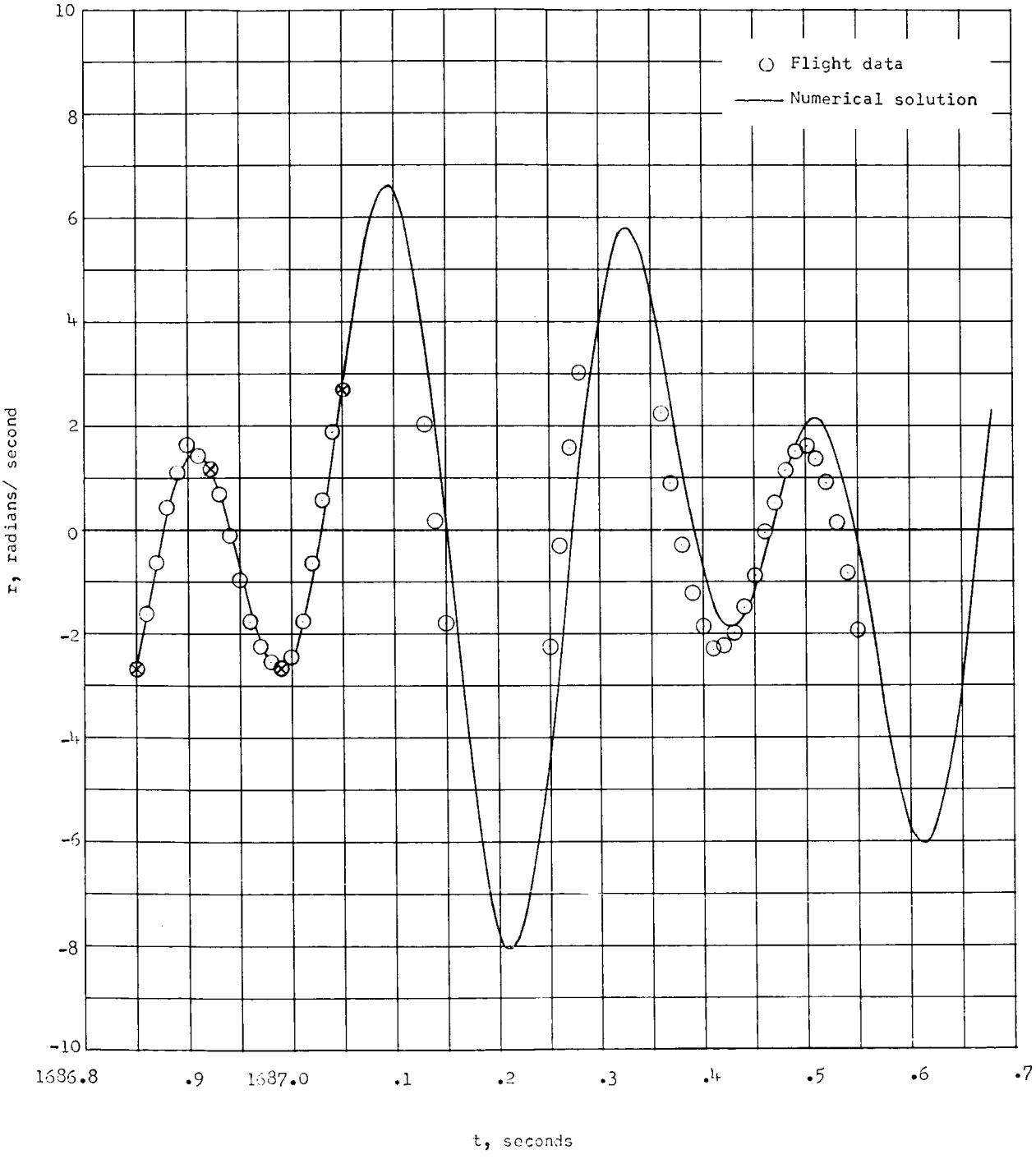

(a) Yaw rates.

Figure 13.- Comparison of computed data with corresponding measured flight data. 1686.85 to 1687.68 seconds. Crossed symbols indicate data points selected for curve-fit program.

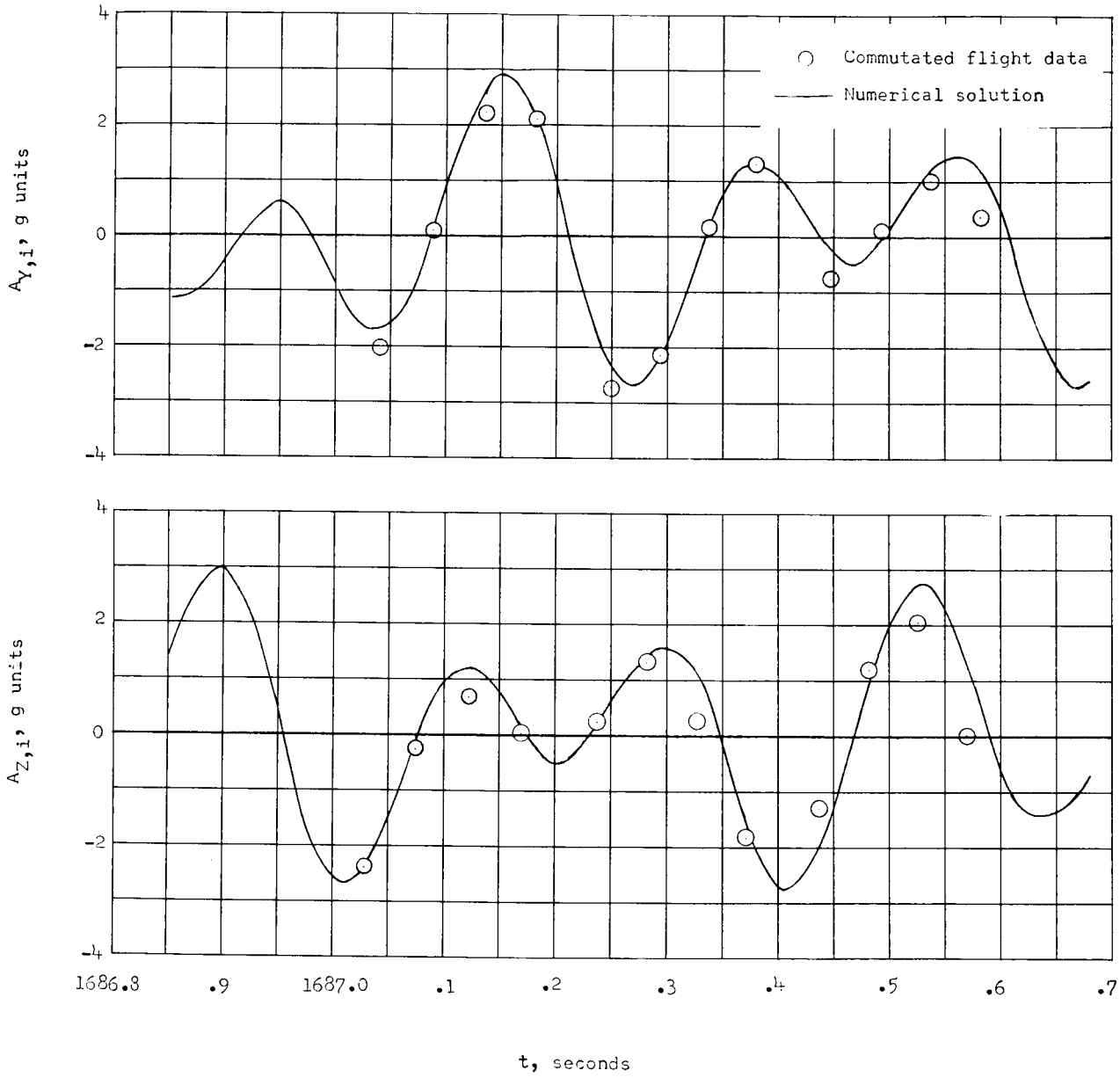

(b) Indicated accelerations.

Figure 13.- Continued.

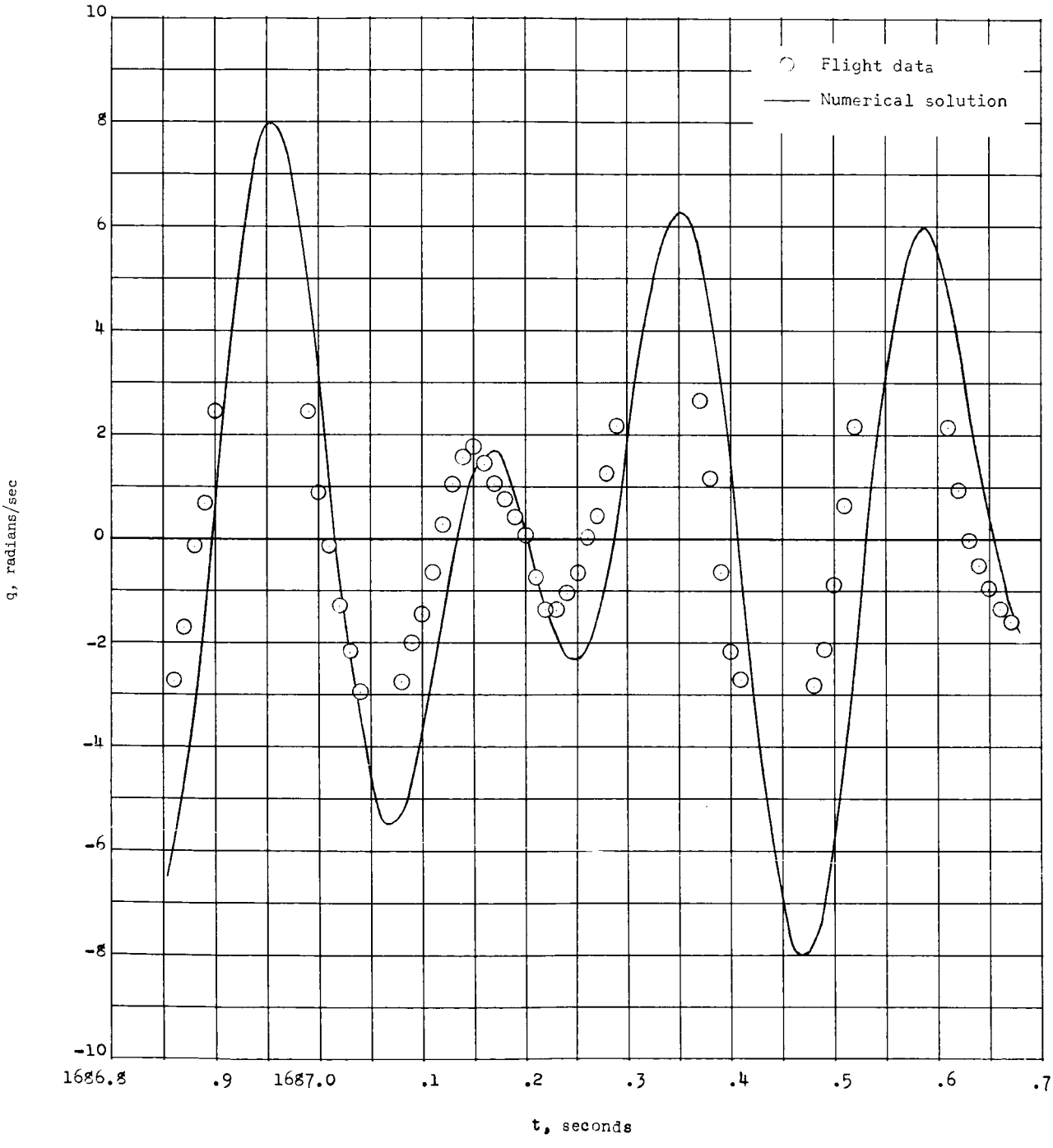

(c) Pitch rates.

Figure 13.- Concluded.

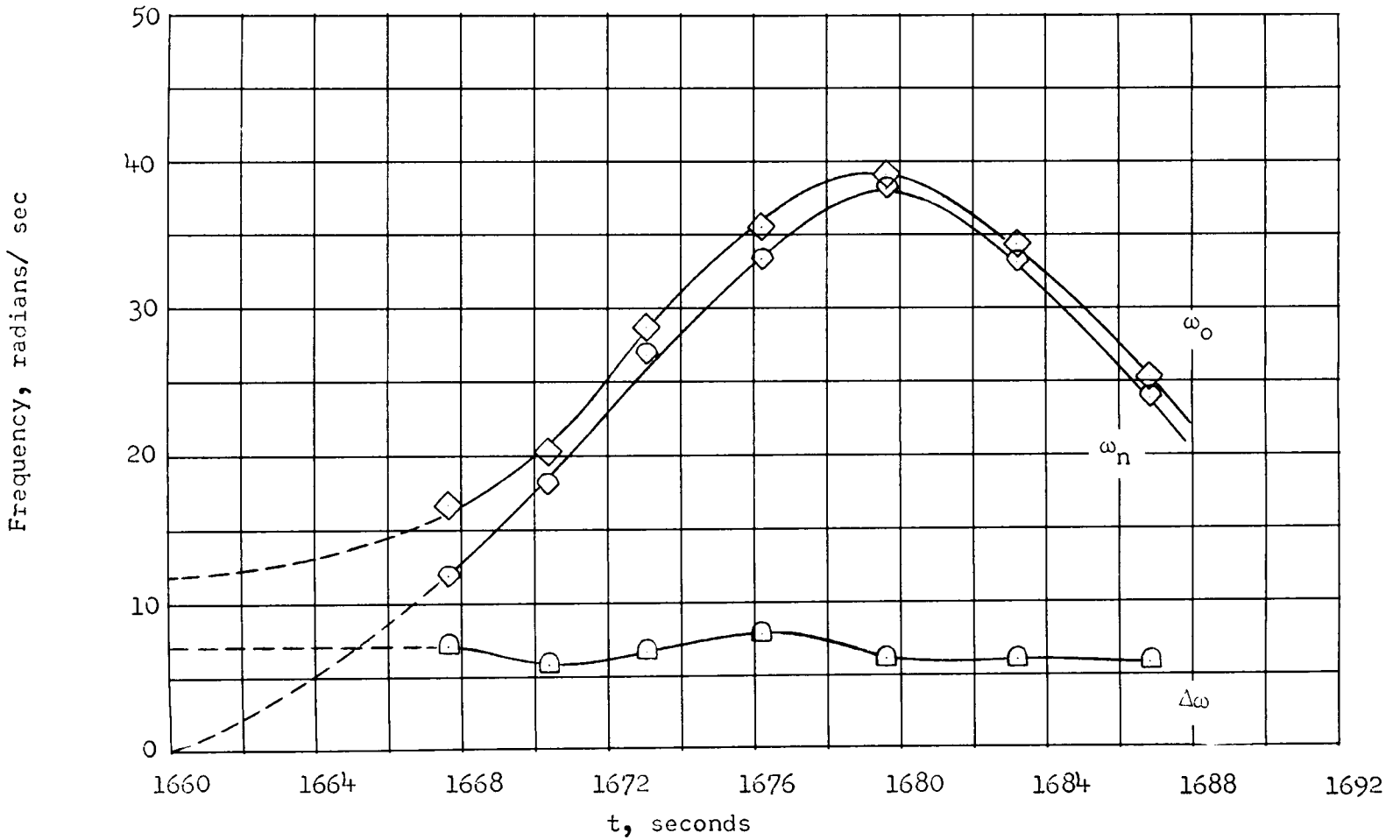

Figure 14.- Time histories of frequency parameters used in simulations. Dashed lines are extrapolations to values in space.

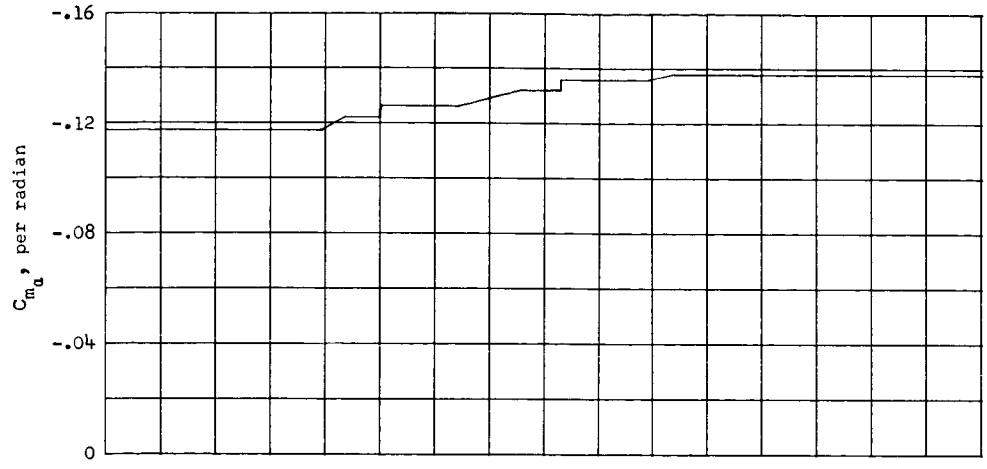

(a) Pitching-moment slope.

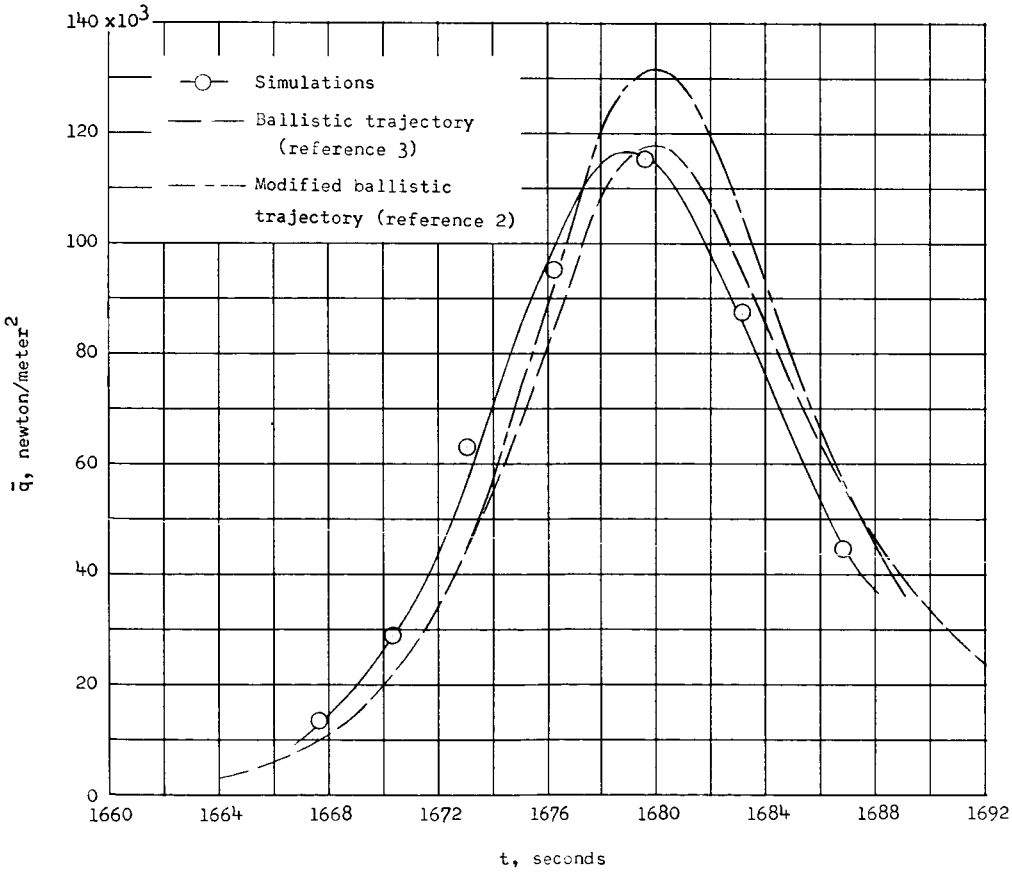

(b) Dynamic pressure.

Figure 15.- Pitching-moment-curve slope time history and corresponding dynamic pressures required for motion simulations compared with dynamic pressures of ballistic trajectories of references 2 and 3.

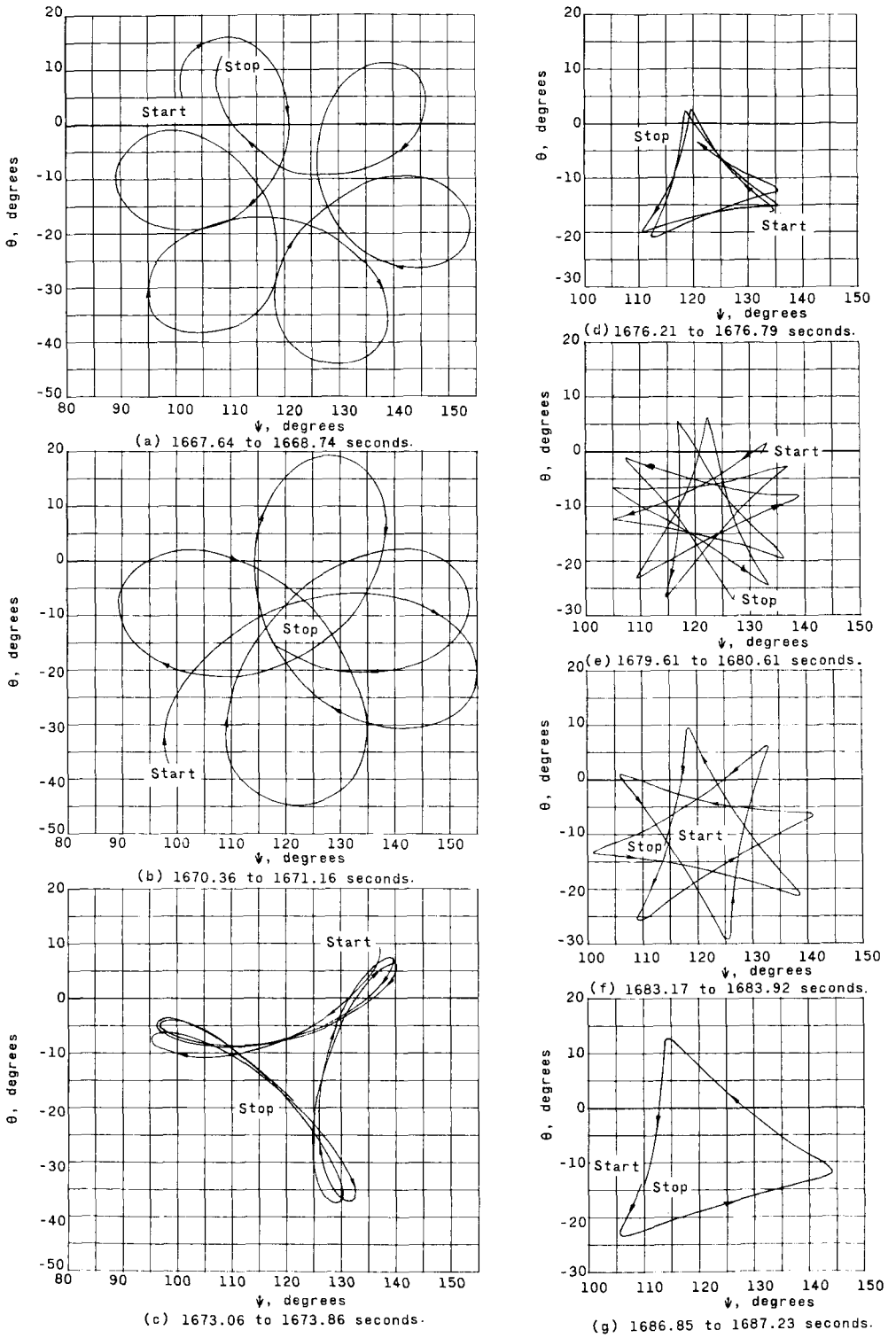

Figure 16.- Comparison of angular-motion patterns in inertial reference plane.

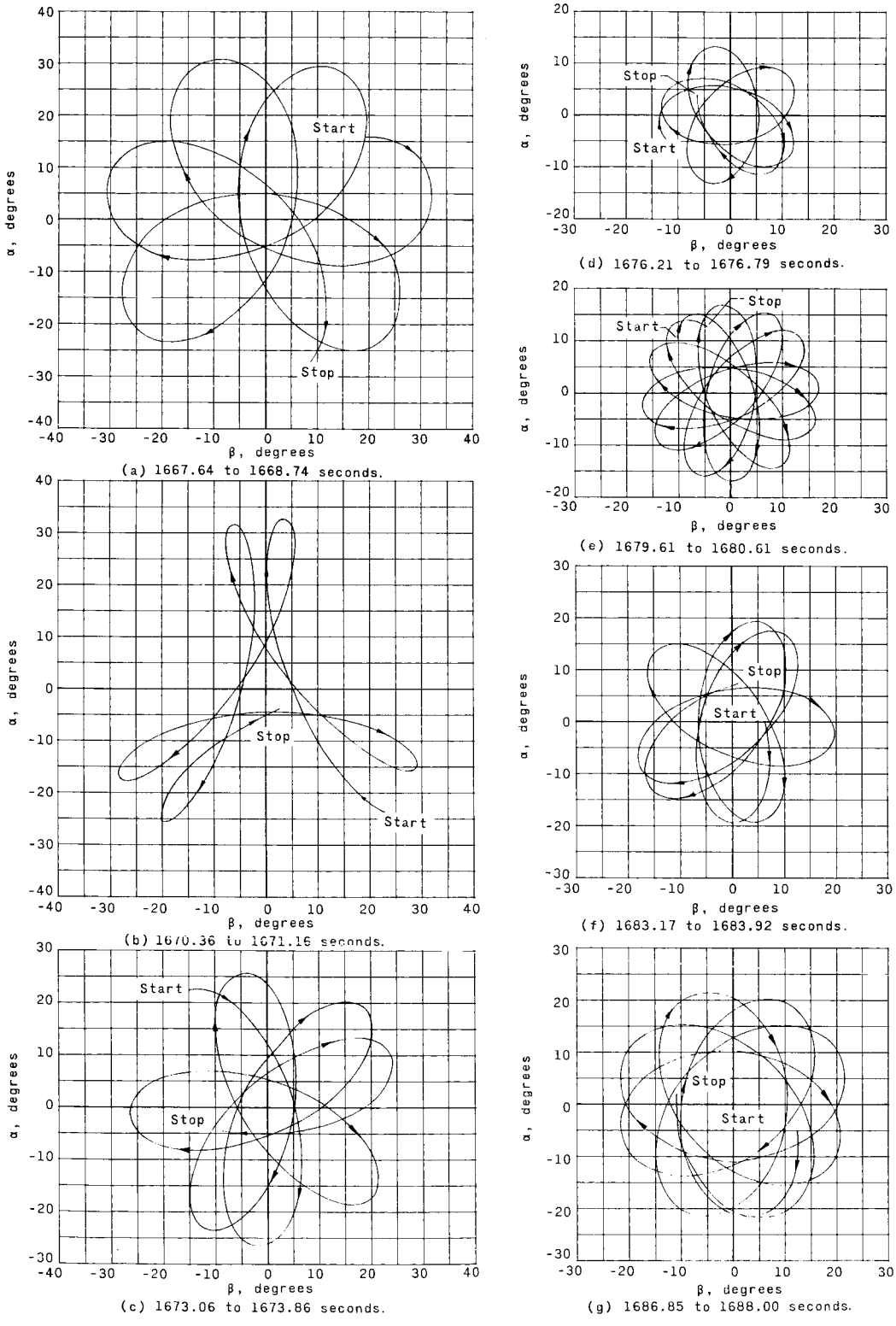

Figure 17.- Comparison of angular-motion patterns in relative reference plane.

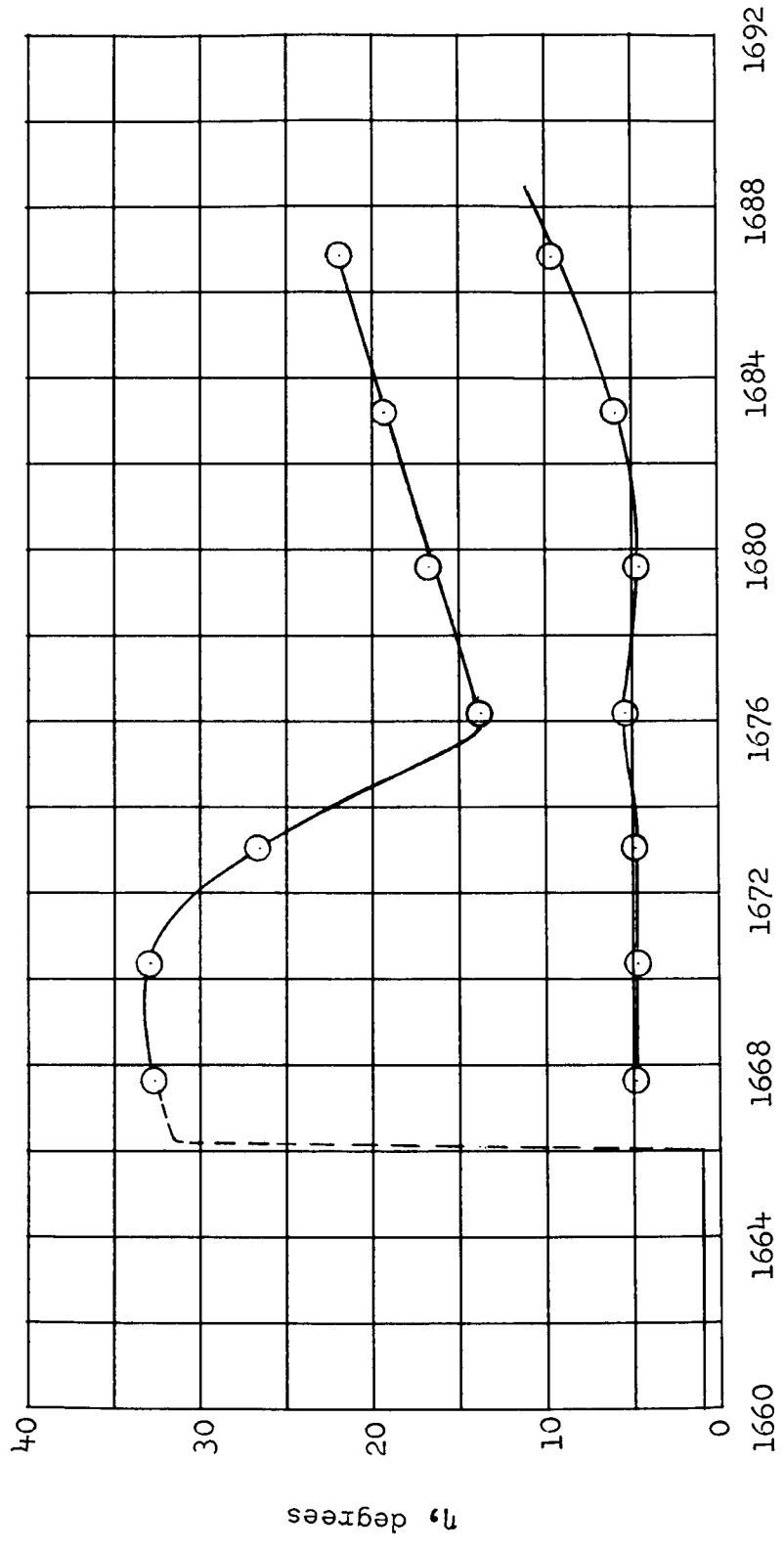

Figure 18.- Envelope of total angle-of-attack time history.

"The aeronautical and space activities of the United States shall be conducted so as to contribute . . . to the expansion of human knowledge of phenomena in the atmosphere and space. The Administration shall provide for the widest practicable and appropriate dissemination of information concerning its activities and the results thereof."

—NATIONAL AERONAUTICS AND SPACE ACT OF 1958

NASA SCIENTIFIC AND TECHNICAL PUBLICATIONS

TECHNICAL REPORTS: Scientific and technical information considered important, complete, and a lasting contribution to existing knowledge.

TECHNICAL NOTES: Information less broad in scope but nevertheless of importance as a contribution to existing knowledge.

TECHNICAL MEMORANDUMS: Information receiving limited distribution because of preliminary data, security classification, or other reasons.

CONTRACTOR REPORTS: Technical information generated in connection with a NASA contract or grant and released under NASA auspices.

TECHNICAL TRANSLATIONS: Information published in a foreign language considered to merit NASA distribution in English.

TECHNICAL REPRINTS: Information derived from NASA activities and initially published in the form of journal articles.

SPECIAL PUBLICATIONS: Information derived from or of value to NASA activities but not necessarily reporting the results of individual NASA-programmed scientific efforts. Publications include conference proceedings, monographs, data compilations, handbooks, sourcebooks, and special bibliographies.

Details on the availability of these publications may be obtained from:

SCIENTIFIC AND TECHNICAL INFORMATION DIVISION

NATIONAL AERONAUTICS AND SPACE ADMINISTRATION

Washington, D.C. 20546